Theoretical Calculation of Core-Excited States Along Dissociative Pathways Beyond Second-order Perturbation Theory

Meng Huang,[†] Chenyang Li,[‡,†] and Francesco A. Evangelista[*,†]

†*Department of Chemistry and Cherry Emerson Center for Scientific Computation, Emory University, Atlanta, Georgia, 30322, U.S.A.*

‡*Key Laboratory of Theoretical and Computational Photochemistry, Ministry of Education, College of Chemistry, Beijing Normal University, Beijing, 100875, China*

E-mail: francesco.evangelista@emory.edu

Abstract

We extend the multireference driven similarity renormalization (MR-DSRG) method to compute core-excited states by combining it with a GASSCF treatment of orbital relaxation and static electron correlation effects. We consider MR-DSRG treatments of dynamical correlation truncated at the level of perturbation theory (DSRG-MRPT2/3) and iterative linearized approximations with one- and two-body operators [MR-LDSRG(2)] in combination with a spin-free exact-two-component (X2C) one-electron treatment of scalar relativistic effects. This approach is calibrated and tested on a series of 16 core-excited states of five closed- and open-shell diatomic molecules containing first-row elements (C, N, and O). All GASSCF-MR-DSRG theories show excellent agreement with experimental adiabatic transitions energies, with mean absolute errors ranging between 0.17 and 0.35 eV, even for the challenging partially

doubly-excited states of the N_2^+ molecule. The vibrational structure of all these transitions, obtained from using a full potential energy scan, shows a mean absolute error as low as 25 meV for DSRG-MRPT2 and 12/13 meV for DSRG-MRPT3 and MR-LDSRG(2). We generally find that a treatment of dynamical correlation that goes beyond the second-order level in perturbation theory improves the accuracy of the potential energy surface, especially in the bond-dissociation region.

1 Introduction

The emergence over the past few decades of new generations of synchrotrons and free-electron lasers has enabled high-resolution and time-resolved X-ray absorption spectroscopy (XAS) to flourish.[1–6] The core-excited states probed via X-ray spectroscopy can shed light on the electronic and geometric structure of molecules, and more importantly, offer a way to follow the dynamics of electrons and nuclei down to the attosecond scale. Interpreting the data produced in these state-of-art XAS experiments requires accurate and cost-effective electronic structure calculations. However, the theoretical modeling of even the simplest diatomic molecules investigated in the earliest high-resolution XAS studies[7,8] already proves to be difficult. Though significant advances have been made in the electronic structure theory and electron dynamics of core-excited states,[3,9,10] an important research direction is expanding existing techniques to open-shell species.

Core excitations are more challenging to characterize computationally than valence excitations. They require an accurate description of polarization and orbital relaxation effects resulting from the creation of a core hole,[9,10] and for elements past the first row, it becomes increasingly important to account for both scalar and spin-orbit relativistic effects.[11–14] A wide range of electronic theories have been developed for core-excited states. Among the most economical and widely applied methods are those based on density functional theory (DFT), including Δ self-consistent-field,[15–20] time-dependent DFT,[21–29] and

transition-potential DFT.[30,31] Wave function methods offer a systematic way to increase the accuracy of core-excited states at the price of higher computational cost. The majority of wave function methods for core-excited states are based on a single-reference formalism and include the static exchange method,[32,33] configuration-interaction based approaches,[34–37] non-orthogonal configuration interaction,[38,39] excited-state mean-field theory,[40] coupled clusters response[41–45] and equation-of-motion theory (EOM-CC),[46–51] and other many-body approaches.[52,53] In many of these approaches, orbital relaxation effects are treated with a linear level instead of infinite order (i.e., by fully relaxing the orbitals or by including the exponential of single excitations). Therefore, it is often the case that the accuracy of core-excitation energies is somewhat inferior to that of valence excitations. The algebraic diagrammatic construction (ADC), which originates in Green's function theory,[54–56] has also seen wide application to core-excited states. In addition, real-time methods including both real-time TDDFT[57–60] as well as real-time EOM-CC[61] theories have also been applied to simulate attosecond electron dynamics and XAS spectra.

In many cases, when a single electronic configuration cannot accurately describe either the ground or core-excited state,[62] it might be necessary to go beyond single reference formalisms. This is, for example, the case when modeling core-excited states of molecules stretched along dissociative pathways, open-shell species, and excited states that have pronounced multideterminantal character. The most common multireference (MR) methods for treating core-excited states include multiconfigurational self-consistent-field (MCSCF) based methods,[63–66] MR configuration interaction,[67–69] and multireference coupled cluster (MRCC) theories.[70–73] Due to the inherent challenges of generalizing multireference methods beyond low-order perturbation theory,[74–76] most applications of MR methods to core-excited states have focused on treating dynamic correlation up to second order.

A convenient way to generate zeroth-order reference wave functions for MR treatments of core-excited states is the restricted active space SCF (RASSCF) method.[77] RASSCF can be used to limit the reference space to determinants with one or more core electrons promoted

to the valence orbitals, avoiding variational collapse to the ground state. RASSCF and RASSCF with second-order perturbative corrections (RASPT2)[78,79] find wide application in the simulation of X-ray spectra and have recently been applied[80,81] to the CO^+ and N_2^+ molecules considered in this work. Other variants of MCSCF related to RASSCF have been applied to study CO and NO.[63,82] MCSCF-based methods have also been widely applied in other systems where single-reference methods fail, such as transition metal complexes both in the gas-phase[65,83–86] and solution.[87,88]

Beyond low-order perturbative theories, there are only few applications of multireference coupled-cluster theories to XAS. Most of the early studies[70–72] computed vertical core excitation energies of small molecules with MRCC truncated to singles and doubles, yielding results that are comparable with single-reference EOM-CC with singles and doubles. More recently, Maganas and co-workers[73] compared the performance of MR-EOM-CC and MRCI theories on metal L-edge XAS, expanding the domain of application of earlier MRCC works.

In this work, we report a strategy to compute core-excited states that combines a generalized-active-space SCF (GASSCF)[89,90] treatment of static correlation with a treatment of dynamical correlation based on the multireference driven similarity renormalization group (MR-DSRG).[91,92] The GASSCF method generalizes the restrictions imposed by the RASSCF method and offers a flexible approach to apply multireference methods to core-excited states. Previous studies that examined the accuracy of multireference perturbation theories based on the DSRG (DSRG-MRPT) showed that a third-order treatment (DSRG-MRPT3) reaches similar accuracy to MRCI with singles and doubles and improves upon its second-order analog (DSRG-MRPT2),[93] an improvement also observed in the case of CAS plus perturbative corrections (CASPT).[94,95] Compared to same-order CASPTn theories ($n = 2, 3$), DSRG-MRPTn methods avoid higher-order density cumulants at the cost of a small loss of accuracy. Other truncated MR-DSRG schemes include the MR-LDSRG(2) method, an iterative approach that accounts for dynamical correlation at the level of single and double excitations (analogous to the CCSD method).[96] Previous benchmark stud-

ies[93,97,98] revealed that the hierarchy of DSRG-MRPT2, DSRG-MRPT3, and MR-LDSRG(2) theories systematically converge energies and properties of ground and valence excited states towards experimental values.

In this study, we test the performance of MR-DSRG methods in computing potential energy curves of core-excited states of diatomic molecules. Specifically, we have computed ground- and core-excited state potential energy curves for five diatomic molecules and determined their corresponding vibrational levels. The article is structured as follows. In Sec. 2 we briefly summarize the GAS and MR-DSRG approaches. In Sec. 3 we provide details of the computations performed in this study. Next, in Sec. 4 we calibrate the calculation parameters (basis set and flow parameter) used in the core-excited computations and test the MR-DSRG methods on the CO, CO^+, N_2, $N_2{}^+$ and NO molecules. The accuracy of core-excited states computed with the MR-DSRG methods is accessed by comparing vertical transition energies and the vibrational structure of sixteen core excitations to the experimental ones. Lastly, in Sec. 5 we summarize the findings of this work and provide a perspective on the application of MR-DSRG methods to the computation of core-excite states of large molecules.

2 Theory

In this section we briefly summarize the main features of MR-DSRG theory and its combination with GASSCF references used to compute core-excited states. The general computational scheme underlying our approach is illustrated in Fig. 1. Here the GASSCF reference provides a zeroth-order description of the ground and core-excited states, while a truncated MR-DSRG method is used to include dynamical correlation effects.

2.1 General Active Spaces References

Our modeling of core-excited states begins by defining a set of GASSCF zeroth-order reference states $\{\Psi_\alpha\}$ that account for orbital relaxation and static correlation in the core and

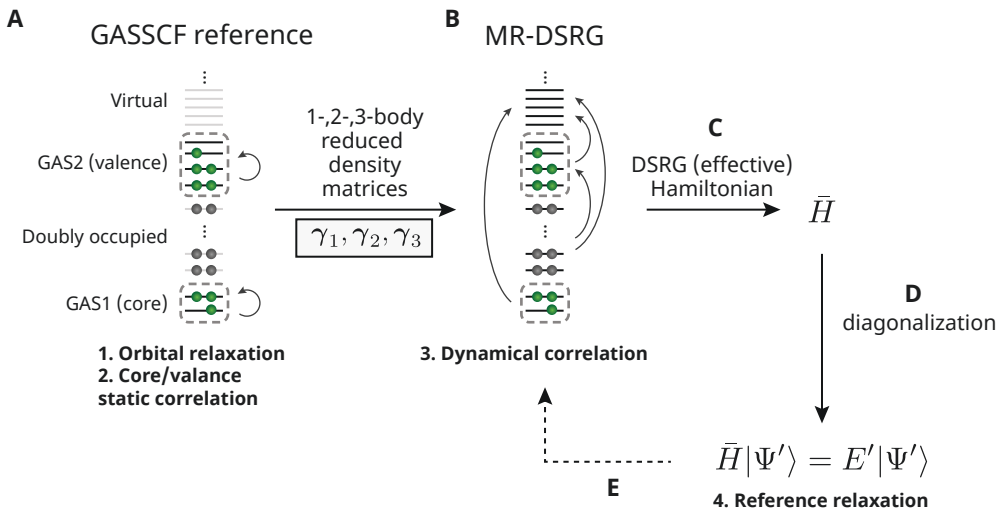

Figure 1: Computational scheme employed to compute core-excited states using a GASSCF reference and multireference DSRG methods. A) A GASSCF reference is used to provide a zeroth-order approximation to a target core excitation (e.g., O K-edge). B) Dynamical correlation effects are added using a truncated MR-DSRG method and the 1-,2-, and 3-body reduced density matrices of the GASSCF reference. C) The converged DSRG amplitudes are used to build the DSRG Hamiltonian ($\bar{H}$). D) Diagonalization of $\bar{H}$ provides the relaxed energy E' and reference Ψ'. E) Optionally, the relaxed reference Ψ' is passed back to the MR-DSRG code and steps B–E are iterated until self consistency is reached.

valence orbitals. In the GAS approach,[89,90] the orbitals are partitioned into core (doubly occupied), active (partially occupied), and virtual (empty), with the active space being further partitioned into a variable number of orbital subspaces (GASn, with $n = 1, 2, \ldots$). Given this partitioning, the determinant space defined by GAS is specified by imposing restrictions on the minimum and maximum number of electrons in each GASn space. Each reference state is a generalized active space self-consistent-field wave function of the form

$$|\Psi_\alpha\rangle = \sum_{\mu}^{\text{GAS}} C_\mu^\alpha |\Phi_\mu\rangle \tag{1}$$

where $|\Phi_\mu\rangle$ is a determinant that satisfies the GAS restrictions and C_μ^α its corresponding coefficient. Compared to the RAS partitioning[77]—which defines only three spaces and imposes restrictions only on the first and last—GAS allows for more flexibility in the definition of the zeroth-order reference.

As shown in Fig. 1, in core-excited state calculations based on GAS wave functions, we include the core orbital(s) from which electrons are excited in the GAS1 space, and enforce the presence of one or more holes depending on the type of excitation targeted. Valence orbitals are included in the GAS2 space (without occupation restrictions), thus allowing to capture core-excited states that have multi-determinantal character. We generally employ different GAS partitionings to describe different core excitations. For example, in modeling the K-edge spectra of CO, we perform separate computations in which only the C 1s or the O 1s orbitals are included in the GAS1 space to simulate excitations from the carbon and oxygen atoms, respectively. The ground electronic state is similarly described by a GAS reference, restricting GAS1 to be fully occupied. We note that for the purpose of this work, the determinants spaces here obtained with a GAS could also be reproduced with the RAS approach with extra restriction on the minimum number of holes in the RAS1 (core orbitals).

2.2 Multireference DSRG treatment of dynamical correlation

The GASSCF zeroth-order references described in the previous section provide a qualitative approximation to core-excited states. To include the missing dynamical correlation effects and reference relaxation effects induced by dynamical correlation, we augment the GASSCF states with the multireference DSRG theory.[91,92,96,98–100] The MR-DSRG is a unitary formalism in which the Hamiltonian $\hat{H}$ is gradually block-diagonalized by a unitary (canonical) transformation:

$$\hat{H} \rightarrow \bar{H}(s) = e^{-\hat{A}(s)} \hat{H} e^{\hat{A}(s)} \tag{2}$$

The operator $\hat{A}(s)$ is anti-Hermitian and it is expressed in terms of a generalized form of the coupled cluster excitation operator $\hat{T}(s)$ as $\hat{A}(s) = \hat{T}(s) - \hat{T}^{\dagger}(s)$. The amplitudes that enter into $\hat{T}(s)$ depend on the number $s \in [0, \infty)$, usually referred to as *flow parameter*. The purpose of this unitary transformation is to eliminate the second-quantized components of $\bar{H}(s)$ that couple active orbitals to the core and virtual spaces. These components of $\bar{H}(s)$

are referred to as non-diagonal, and are indicated with $\bar{H}^N(s)$. When this decoupling is achieved exactly [i.e., $\bar{H}^N(s) = 0$], one can obtain the exact eigenvalues for a manifold of states by diagonalizing $\bar{H}(s)$ in the space of CAS determinants.

One of the challenges associated with the block-diagonalization of the Hamiltonian via Eq. (2) is the appearance of numerical instabilities. These are related to excitations with small energy denominators, which, in perturbation theory lead to divergences of the dynamical correlation energy (the intruder state problem). To avoid intruders, the DSRG seeks only a partial block-diagonalization of the Hamiltonian by solving the following modified equation

$$\bar{H}^N(s) = \hat{R}(s) \tag{3}$$

The *source* operator $\hat{R}(s)$ regularizes excitations with small denominators, and the flow parameter s determines to which extent excitations are suppressed. This statement has a precise interpretation in perturbative truncation schemes based on the MR-DSRG:[93] excitations with denominators Δ less than the energy cutoff $\Lambda = 1/\sqrt{s}$ are suppressed (and are equal to zero when $\Delta = 0$), while excitations with $\Delta \gg \Lambda$ are nearly-identical to those obtained from the corresponding unregularized equations. The detailed form of the source operator is reported in Appendix A.

Once the DSRG equation [Eq. (3)] is solved, the energy is given by one of the eigenvalues of the DSRG Hamiltonian [$\bar{H}(s)$] in the space of GAS determinants

$$\bar{H}(s)\,|\Psi'\rangle = E'(s)\,|\Psi'\rangle \tag{4}$$

where $E'(s)$ and $|\Psi'\rangle$ are the *relaxed* energy and reference, respectively. The relaxed energy includes contributions from dynamical correlation plus reference relaxation effects. It is also possible to obtain a *fully relaxed* energy, whereby Eqs. (3) and (4) are solved iteratively until self consistency is reached. The formalism described here is state-specific, in the sense that the operator $\hat{T}(s)$ is optimized for a single electronic state. For near-degenerate electronic

states of the same symmetry, we instead employ a state-averaged version of the MR-DSRG that allows to compute more than one state at a time.[93]

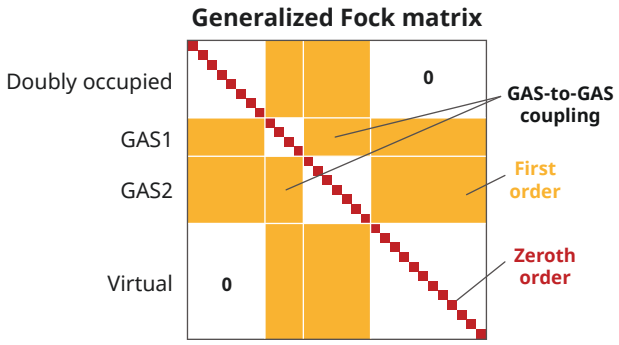

Figure 2: Structure of the generalized Fock matrix for a GASSCF state defined by two GAS spaces.

In this work we consider both perturbative and iterative approximations to the MR-DSRG. Partitioning the Hamiltonian into a zeroth- plus first-order component, the DSRG equation and the DSRG energy can be expanded order-by-order into closed expression. To define the zeroth-order Hamiltonian, we consider the generalized Fock matrix:

$$f_q^p = h_q^p + \sum_{jk} \langle pj \| qk \rangle \gamma_k^j \tag{5}$$

defined in terms of the one-electron integrals (h_q^p), antisymmetrized two-electron integrals ($\langle pj \| qk \rangle$), and the one-body reduced density matrix of the reference state (γ_k^j). For convenience, we work in a semi-canonical basis in which the generalized Fock matrix is diagonal in each orbital space (doubly occupied, GAS1, GAS2, ...). For a GASSCF reference, the matrix f_q^p in the semi-canonical basis has the structure shown in Fig. 2.

We take the zeroth-order Hamiltonian to be the diagonal component of the generalized Fock matrix

$$\hat{H}^{(0)} = \sum_p \epsilon_p \{\hat{a}_p \hat{a}_p^\dagger\} \tag{6}$$

where the quantities $\epsilon_p = f_p^p$ are diagonal elements of the generalized Fock matrix. Truncation of the MR-DSRG using this partitioning leads to second- and third-order DSRG

multireference perturbation theories (DSRG-MRPTn, $n = 2, 3$). Detailed derivations of these methods are reported in Refs. 99 and 100 and we encourage the reader to consult those works for further details.

It is important to note one difference between the current formulation of the DSRG-MRPTn methods based on a GAS reference and a complete active space, as reported previously.[99] In the case of CAS references, there are no first-order one-body terms that couple active orbitals, and consequently, the first-order correlation energy is null. Instead, with our choice of $\hat{H}_0$, the perturbation contains off-diagonal one-body terms (see Fig. 1) that introduce GAS-to-GAS internal excitations and a corresponding first-order energy correction. These first-order corrections correspond to excitations from core to valence orbitals, and are currently neglected in the present implementation. In the case of core-excited states, neglecting internal GAS-to-GAS excitations may be justified using a perturbative argument on the basis of the large difference in the energy between the core and valence orbitals. An alternative solution to the one adopted here would be to semicanonicalize the union of all GAS blocks of the generalized Fock matrix. This, would however, cause a mixing of orbitals in different GAS spaces and change the reference energy.

We also consider treatments that go beyond perturbation theory, specifically, the linearized MR-DSRG approach with one- and two-body operators [MR-LDSRG(2)].[96] In the MR-LDSRG(2), $\hat{A}(s)$ is truncated to one- and two-body operators [$\hat{A}(s) \approx \hat{A}_1(s) + \hat{A}_2(s)$] and the DSRG Hamiltonian is computed as a series of commutators using the Baker–Campbell–Hausdorff (BCH) formula

$$\begin{aligned} \bar{H}_{1,2}(s) =& \hat{H} + [\hat{H}, \hat{A}(s)]_{1,2} \\ &+ \frac{1}{2}[[\hat{H}, \hat{A}(s)]_{1,2}, \hat{A}(s)]_{1,2} + \dots \end{aligned} \tag{7}$$

The notation $[\cdot, \cdot]_{1,2}$ means that the operator resulting from the commutator is truncated to its one- and two-body components. Note that the presence of both excitation and de-excitation operators in $\hat{A}(s)$ makes the BCH expansion of the DSRG Hamiltonian a non-

truncating series. In practice, this series is truncated when the norm of the last term is less than a threshold, yielding in general a total of 10–15 terms. The MR-LDSRG(2) truncation scheme is similar to the unitary coupled-cluster with singles and doubles scheme (although it is only complete up to second order), and the resulting DSRG Hamiltonian contains up to two-body interactions, as the original Hamiltonian. Like for the DSRG-MRPTn methods, we exclude from $\hat{A}$ those operator components that correspond to GAS-to-GAS excitations.

3 Computational Details

As part of this work, we implemented both GASSCF and GAS-based variants of the MR-DSRG methods in `Forte`,[101] an open-source plugin for the `Psi4` *ab initio* quantum chemistry package.[102] Our recent implementation of spin-free MR-DSRG theories[98] enables these GAS based MR-DSRG calculations on open-shell molecules. The GASSCF-MR-DSRG calculations are performed according to the following procedure. First, ground-state molecular orbitals are obtained using restricted Hartree–Fock (RHF) using a spin-free exact-two-component (X2C) one-electron treatment of scalar relativistic effects.[103] In this work we have tested a variety of basis sets, including the correlation-consistent polarized valence set (cc-pVXZ) optimized for Douglass–Kroll (DK) relativistic Hamiltonians (cc-pVXZ-DK) (X=D,T,Q),[104,105] cc-pVXZ-DK augmented with diffuse functions (aug-cc-pVXZ-DK, X=D,T,Q),[104–107] cc-pVXZ and cc-pVXZ-DK basis set augmented with core functions (cc-pCVXZ/cc-pCVXZ-DK),[104–106] the def2-XZVP (X=T,Q),[108,109] and ANO-RCC-XZVP (X=T,Q).[110]

For molecules like N_2^+ with partially occupied π orbitals, orbital degeneracy is enforced by performing a state-averaged CASSCF (SA-CASSCF) calculation using as an active space that includes all valence and core orbitals of both atoms. Next, these initial molecular orbitals are optimized using GASSCF theory where the active spaces are separated into multiple GAS and the number of electrons in each GAS is constrained. The active space in this GASSCF step is also formed by all the valence and core orbitals, i.e., $1s$, $2s$ and $2p$

orbitals for second period elements. Depending on whether or not two nuclei of the molecule are identical, the active space is separated into two GAS differently. For CO, CO^+, and NO, one core level is selected for each atom from which the electron is excited and included in the GAS1 space, while all other active orbitals belong to the GAS2 space. In the case of N_2 and N_2^+, the lowest two molecular orbitals (corresponding to in- and out-of-phase combinations of 1s orbitals) form the GAS1 space, and the rest of the orbitals belong to the GAS2 space. The number of electrons in GAS1 is always $2n$ for the ground state and $2n-1$ for the electronic state where n is the number of GAS1 orbitals. To simplify the discussion, we use the notation $(n_{\mathrm{o}}^1\mathrm{o}, n_{\mathrm{e}}^1\mathrm{e}; n_{\mathrm{o}}^2\mathrm{o}, n_{\mathrm{e}}^2\mathrm{e}; \cdots)$ to represent a specific distribution of electrons in GAS where n_{o}^m and n_{e}^m are the number of orbitals and the number of electrons in the m-th GAS space. For example, the GAS for the ground and core-excited electronic states of $N_2{}^+$ under this notation are (2o,4e;8o,5e) and (2o,3e;8o,6e), respectively. We note for the cases discussed in this work each GAS space has a constant number of electrons; however, our GAS implementation is general, such that restrictions on the minimum and maximum number of electrons can also be applied to each GAS.

For all transitions, state-specific GASSCF computations are performed on each electronic state, unless two core-excited states undergo mixing due to strong coupling along the potential curve. We found this to be the case for two $1s_{\mathrm{C}}^1 5\sigma^1 2\pi^1$ states of CO^+, two $1s_{\mathrm{O}}^1 5\sigma^1 2\pi^1$ states of CO^+, two $1\sigma_u^1 3\sigma_g^1 1\pi_g^1$ states of N_2^+, and three $1s_{\mathrm{O}}^1 2\pi^1$ states of NO. Finally, using the optimized GASSCF MOs for each electronic state, DSRG-MRPT2, DSRG-MRPT3 and MR-LDSRG(2) levels of theories are applied to account for dynamical electron correlation. State-average MR-DSRG (SA-MR-DSRG)[93] calculations are performed if the electronic states are obtained with SA-GASSCF. In all DSRG computations, a one-step reference relaxation correction is computed, in a manner consistent with state averaging or state specific calculations.

The current code GASSCF-MR-DSRG computations assumes several approximations. First, orbital rotations between two different GAS are frozen to prevent the collapse of a

core-excited state to the ground state. This approximation has been widely used in the core-excited state calculation based on RASSCF optimizations.[65,80,81,84] Second, the number of electrons within each GAS is frozen in both the ground and excited state calculations. This approximation neglects the coupling between core-excited determinants and all other determinants, and leads to a difference in the vertical transition energy for about 50 meV near the equilibrium geometry. This energy difference may increase to 100 meV as a bond is stretched, but preliminary tests show that including these couplings has only little effect (less than 1 %) on the final vibrational Franck–Condon factors. Therefore, this term is ignored in our calculations to significantly decrease the number of determinants involved in the GASSCF step. Last, internal amplitudes that correspond to electron excitations between different GAS spaces are ignored in the MR-DSRG treatment. This approximation generally leads to a tiny correction to the transition energy, for example, of around 2 meV for N_2^+. These three approximations can be justified using a perturbation theory argument and the large energy difference between orbitals from different GASs.

The vibronic spectra of all core-excited transitions are then calculated from potential energy scans on both ground and excited electronic states that range from the equilibrium geometry to the bond-dissociation region. The potential scans use uniform grid with a spacing of 0.05 Å. Tests on a denser grid with 0.01 Å spacing show that the Franck–Condon factors change at most by 1%. The equilibrium geometry of each electronic state is computed from a cubic spline potential fitted to energies evaluated on a grid of 0.001 Å spacing.

Using these potentials, the vibrational eigenvalues and eigenvectors are then obtained using the discrete variable representation (DVR) method[111,112] with the values of potential energy at each grid points evaluated through cubic spline interpolation. The intensity of the vibronic spectrum peaks are approximated with the corresponding Franck–Condon factors, which are obtained by computing the overlap of the ground and excited vibrational eigenvectors and ignoring the nuclear dependence of the transition dipole moment. All spectra are simulated at a vibrational temperature set to 0 K. All core-valence separated ADC (CVS-

ADC) results reported in this work were computed using `Psi4`[102] and `adcc` package.[113,114] All core-valence-separated coupled cluster singles and doubles (CVS-EOM-CCSD) results reported in this work were computed using a modified version of the `CFOUR` package.[115–117]

4 Result and Discussion

4.1 Basis set and flow parameter choice

To test the accuracy of core excitation energies computed with the GASSCF-MR-DSRG approach, we compute a total of 16 K-edge transitions for CO, CO^+, NO, N_2, and N_2^+. These systems comprise both open- and closed-shell molecules and their high-resolution, vibrationally resolved core-excited transitions have been studied both experimentally and theoretically.[8,63,80–82,118–124] To calibrate the GASSCF-MR-DSRG approach, we begin by studying the sensitivity of core-excited transitions to the choice of basis set. For this purpose, we report adiabatic transition energies (the electronic energy difference between the equilibrium geometries of two states) for the $1\sigma_u \rightarrow 3\sigma_g$ transition of N_2^+ computed with the DSRG-MRPT2 method and a variety of basis sets. In these calculations, the same experimentally-determined molecular geometries[81,125] are used for all basis functions (r_{NN} = 1.116 and 1.076 Å for the ground and core-excited states, respectively). Adiabatic transition energies (T_{e}) and the number of basis functions (N_{b}) for each basis set are listed in Table 1. Complete basis set adiabatic transition energies for the Dunning basis sets were obtained by extrapolation, following previous studies.[126–128] The GASSCF energies (E_X^{SCF}) and the DSRG-MRPT2 correlation energies (E_X^{corr}) for each state were fitted to the equations $E_X^{\mathrm{SCF}} = E_\infty^{\mathrm{SCF}} + A\exp(-bX)$ and $E_X^{\mathrm{corr}} = E_\infty^{\mathrm{corr}} + C/X^3$ (where $X = 3$ for a triple-zeta basis, etc.), respectively, and extrapolated to obtain the corresponding values in the limit of an infinite basis (E_∞^{SCF} and E_∞^{corr}).

In analyzing the different basis set choices, we take as a reference transition energy the extrapolated cc-pCVXZ-DK value (394.49 eV). This value is in good agreement with the

energy computed with the largest two basis sets: a fully decontracted cc-pCVQZ-DK basis (394.49 eV) and the cc-pCVQZ-DK basis augmented with diffuse functions (394.53 eV). We generally find that double-ζ basis sets are insufficiently accurate, overestimating transition energies by as much as 2–3 eV. Basis sets that do not include core-valence functions (cc-pVXZ-DK, ANO-RCC-VXZP, def2-XZVP) generally underestimate transition energies even at the quadruple-ζ level. In particular, the def2-QZVP basis, which lacks core functions and is designed for non-relativistic computations, underestimates T_e by as much as 0.66 eV. Comparing the cc-pCVQZ and cc-pCVQZ-DK results, the X2C relativistic effects amount to a correction of 0.2 eV, as expected for first-row elements. Note that a similar correction is observed if this comparison is performed using the cc-pCVQZ-DK basis in both the non-relativistic and X2C computations. This analysis shows that the cc-pCVQZ-DK offers a good compromise between accuracy and cost for highly-accurate computations, deviating from the reference value by only 0.03 eV. Therefore, all of the results following this section will assume a cc-pCVQZ-DK basis with an X2C treatment of relativistic effects.

A second aspect we investigate is the sensitivity of the computed transition energies with respect to the DSRG flow parameter s. In Table 2 we report excitation energies for the $1\sigma_u \rightarrow 3\sigma_g$ transition of N_2^+ computed with different MR-DSRG treatments of dynamical correlation and flow parameter values in the range 0.25–4 E_h^{-2}. For all MR-DSRG methods, transition energies show a very small dependence on the value of s, until it reaches a relatively large value ($s = 2\ E_\mathrm{h}^{-2}$) where the MR-LDSRG(2) computations fail to converge. The lack of convergence of the MR-LDSRG(2) method for large values of s has been previously observed; however, the best way to address this issue still remains an open question in the context of MR-DSRG theory. The fluctuation of the adiabatic excitation energy for DSRG-MRPT3 and DSRG-MRPT2 is within 0.1 eV, which is comparable to the energy correction from spin-free relativistic effects.

We also note a similar sensitivity for the adiabatic excitation energy for the lowest sulphur K-edge line in CS. In this heavier analog of CO, relativistic effects will be significantly larger

Table 1: Adiabatic transition energy (T_e) and basis set size (N_b) for the $1\sigma_u \rightarrow 3\sigma_g$ transition of the N_2^+ ion calculated with GASSCF-DSRG-MRPT2 and different basis sets. Unless otherwise noted, all results are obtained with a one-electron spin-free X2C Hamiltonian.

Basis Set	N_b	T_e (eV)
cc-pCVDZ-DK	36	396.74
cc-pCVTZ-DK	86	394.65
cc-pCVQZ-DK	168	394.52
CBS/cc-pCVXZ-DK	–	**394.49**
cc-pCVDZ-DK (decontracted)	60	395.34
cc-pCVTZ-DK (decontracted)	110	394.67
cc-pCVQZ-DK (decontracted)	194	394.49
aug-cc-pCVDZ-DK	54	396.69
aug-cc-pCVTZ-DK	118	394.65
aug-cc-pCVQZ-DK	218	394.53
cc-pCVDZ[a]	36	396.54
cc-pCVTZ[a]	86	394.45
cc-pCVQZ[a]	168	394.31
cc-pVDZ-DK	28	397.59
cc-pVTZ-DK	60	394.31
cc-pVQZ-DK	110	394.14
ANO-RCC-VTZP	60	394.55
ANO-RCC-VQZP	110	394.06
def2-TZVP[a]	62	394.46
def2-QZVP[a]	114	393.83

[a] Results obtained with a non-relativistic Hamiltonian.

than the fluctuation introduced by the choice of s.

Due to the low sensitivity of the results with respect to s, in this study we use $s = 0.5$ E_h^{-2}, the optimal empirical choice determined in previous studies.[96,100] The optimal value of s can be different for molecules containing heavier atoms, as shown in our previous study[98] on spin splittings of iron complexes. All MR-LDSRG(2) computations reported in this work were obtained using this value of s without encountering convergence issues.

Table 2: Dependence of the adiabatic transition energies for $1\sigma_u \rightarrow 3\sigma_g$ of N_2^+ ion as a function of the flow parameter s. Results were calculated with a GASSCF reference and various levels of theory [PT2 = DSRG-MRPT2, PT3 = DSRG-MRPT3, LDSRG(2) = MR-LDSRG(2)] using the cc-pCVQZ-DK basis and a spin-free X2C 1-electron treatment of scalar relativistic effects.

s	T_e (PT2) (eV)	T_e (PT3) (eV)	T_e(LDSRG(2)) (eV)
0.25	394.54	394.76	394.65
0.5	394.51	394.75	394.64
1.0	394.53	394.71	394.59
2.0	394.52	394.67	–[a]
4.0	394.47	394.65	–[a]

[a] MR-LDSRG(2) computation on the ground state failed to converge.

4.2 Adiabatic transition energies

Next, we assess the effect of different MR-DSRG treatments of dynamical electron correlation on the computed adiabatic transition energies. In Fig. 3 we plot the potential energy curve of the ground and the $1s_\mathrm{O} \rightarrow 2\pi$ excited state of CO. This example shows very good agreement between all treatments of dynamical correlation, especially beyond second order, with the DSRG-MRPT3 potential energy curve differing consistently from the MR-LDSRG(2) one only by 0.13–0.17 eV in the core excited state and 0.06–0.10 eV in the ground state. This level of agreement is consistent with our previous calculations on the valence-valence transition energies using DSRG theories.[100] In contrast, the DSRG-MRPT2 shows considerable deviations in the potential energy curves, especially in the ground state where the absolute difference with respect to the MR-LDSRG(2) energy at the equilibrium geometry is as large

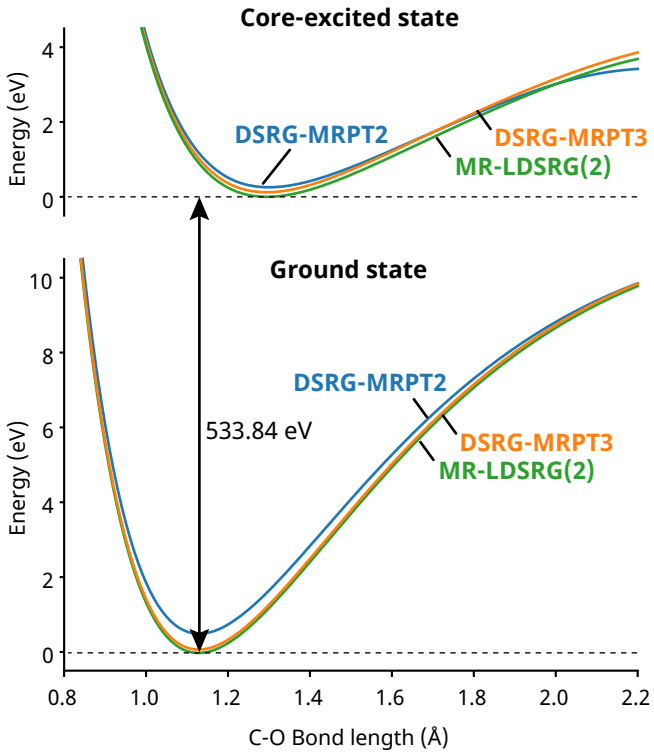

Figure 3: The potential energy surface for the (a) $1s^1_O 2\pi^1$ state and (b) ground state of CO calculated using GASSCF-MR-DSRG level of theory and cc-pCVQZ-DK basis. All the curves are shifted so that the values of MR-LDSRG(2) potential energy in both traces at each minimum are zero.

as 0.5 eV, and only 0.26 eV in the core-excited state.

The trends illustrated for the CO example are generally observed for all computed transitions. Table 3 lists T_e values from different level of GASSCF-MR-DSRG theory as well as the corresponding experimental values. Experimental T_e values do not include zero-point vibrational contributions, and in certain cases were obtained from zero-point corrected electronic energies, T_0, using the experimental zero-point energy. The absolute value for these zero-point vibrational energy corrections are small (typically around 0.05 eV). As can be seen from Table 3, the MR-DSRG predictions are in good agreement with experiment, showing a mean absolute error (MAE) less than 0.4 eV in energy for all methods. Among the three GASSCF-MR-DSRG theories, DSRG-MRPT2 yields a MAE of just 0.17 eV, nearly half the MAEs of the more expensive DSRG-MRPT3 and MR-LDSRG(2) methods. The better performance of the DSRG-MRPT2 is likely due to fortuitous error cancellation. The

Table 3: Adiabatic transition energies (in eV) for the five diatomic molecules reported as deviations from the experiment values. Results were calculated with a GASSCF reference and various levels of theory [PT2 = DSRG-MRPT2, PT3 = DSRG-MRPT3, LDSRG(2) = MR-LDSRG(2)] using the cc-pCVQZ-DK basis and a spin-free X2C 1-electron treatment of scalar relativistic effects.

Excitation	T_e(Exp.)	Error(GASSCF)	Error(DSRG)		
			PT2	PT3	LDSRG(2)
CO, $1s_C \rightarrow 2\pi$	287.41[a]	2.24	–0.01	0.28	0.30
CO, $1s_O \rightarrow 2\pi$	533.62[b]	2.38	–0.04	0.25	0.22
N_2, $1\sigma_u \rightarrow 3\sigma_g$	400.76[c]	3.72	0.13	0.75	0.64
CO^+, $1s_C \rightarrow 5\sigma$	282.00[d]	1.56	0.34	0.25	0.20
CO^+, $1s_C \rightarrow 2\pi$(L)	289.85[d]	2.19	0.10	0.36	0.35
CO^+, $1s_O \rightarrow 5\sigma$	528.48[d]	1.79	0.49	0.44	0.36
CO^+, $1s_O \rightarrow 2\pi$(L)	533.44[d]	2.54	0.36	0.54	0.51
N_2^+, $1\sigma_u \rightarrow 3\sigma_g$	394.28[e]	2.41	0.24	0.36	0.25
N_2^+, $1\sigma_u \rightarrow 1\pi_g$(L)	402.24[e]	2.98	–0.22	0.23	0.19
N_2^+, $1\sigma_u \rightarrow 1\pi_g$(H)	403.11[e]	3.61	0.19	0.69	0.63
NO, $1s_N \rightarrow 2\pi(^2\Delta)$	399.40[f]	1.94	0.15	0.31	0.28
NO, $1s_N \rightarrow 2\pi(^2\Sigma^-)$	399.69[f]	1.98	0.22	0.40	0.37
NO, $1s_N \rightarrow 2\pi(^2\Sigma^+)$	400.01[f]	1.82	0.14	0.33	0.30
NO, $1s_O \rightarrow 2\pi(^2\Sigma^-)$	531.53[b]	1.58	–0.01	0.10	0.06
NO, $1s_O \rightarrow 2\pi(^2\Delta)$	532.64[b]	1.97	0.02	0.13	0.08
NO, $1s_O \rightarrow 2\pi(^2\Sigma^+)$	533.56[b]	1.77	0.00	0.19	0.14
MAE		2.28	0.17	0.35	0.31
MSE		5.60	0.05	0.12	0.10

[a] From Ref. 121.
[b] From Ref. 123.
[c] From Ref. 129.
[d] From Ref. 80.
[e] From Ref. 81.
[f] From Ref. 124.

small error displayed by all the MR-DSRG methods is a significant improvement from the GASSCF theory with a MAE of 2.28 eV, which indicates the dynamic correlation is crucial to achieve sub-eV accuracy in X-ray computations. However, it is necessary to combine both orbital optimization and a multireference treatment of dynamic correlation to achieve high accuracy, as shown, for example, by GASCI-DSRG-MRPT2 computations based on ground state Hartree–Fock orbitals, which yield T_e values with a higher MAE (1.02 eV).

The excellent agreement of GASSCF-MR-DSRG methods with experiment is found to be better than other many-body methods like core-valence separated algebraic-diagrammatic-construction (CVS-ADC) or core-valence separated equation-of-motion coupled cluster theories (CVS-EOM-CC), as seen from the adiabatic transition energies listed in Table 4. Among the three CVS-ADC theories, the CVS-ADC(2)-x method shows the overall best agreement compared with experiment, which is consistent with a previous study.[56] The error at the CVS-EOM-CCSD level is generally between 1–3 eV from experiment, which agrees with previous benchmark studies on the K-edge ionization energies of first-row elements.[116] Although the ADC and EOM-CCSD results show slightly higher errors than the GASSCF-MR-DSRG results, it is important to highlight that these single-reference methods are simpler to use (they do not require selecting an active space) and have a wide applicability range in terms of molecular size due to their efficient implementation.

However, we have found that potential energy scans using CVS-ADC and EOM-CCSD theories lead to qualitatively incorrect curves in the bond-dissociation region and may contain artificial "humps."

The accuracy observed for the MR-DSRG methods is also comparable to other multireference theories. For example, a recent study from Lindblad and co-workers[81] computed transition energies for N_2^+ using MS-RASPT2, and obtained a MAE of 0.46 eV for three transitions (unshifted), while GASSCF-MR-DSRG yields MAEs for the same transitions in the range 0.22–0.43 eV. For the CO^+, the MR-DSRG T_e values have a MAE in the range 0.32–0.40 eV, which are slightly larger than the 0.24 eV MAE for the (unshifted)

MS-RASPT2 data by Couto et al.[80] We note that their study used an imaginary shift of 0.3 E_h to avoid intruder states, a problem addressed in MR-DSRG theories by regularization of the equations via the source operator. For the neutral molecules CO and NO, the predicted adiabatic transition energies from DSRG-MRPT2 theory differ at most by 0.1 eV from those computed with the multi-configurdational coupled electron pair approach (MCCEPA)[82,123] based on an inner-shell CASSCF reference (CASSCF combined with restricted occupation of the inner shell orbitals).[63]

Another important metric to evaluate the accuracy of a theoretical treatment is the energy splitting between core-excited states, which reflects the accuracy with which a method predicts the peak structure of NEXAS spectra. In Table 5 we report a comparison of experimental and calculated adiabatic energy splittings. Energy splittings are in excellent agreement with experimental values, with MAEs less than 0.15 eV for all three MR-DSRG treatments of dynamical correlation. This data again shows no significant improvements when going from DSRG-MRPT2 to the DSRG-MRPT3 and MR-LDSRG(2) results.

4.3 Vibrational features

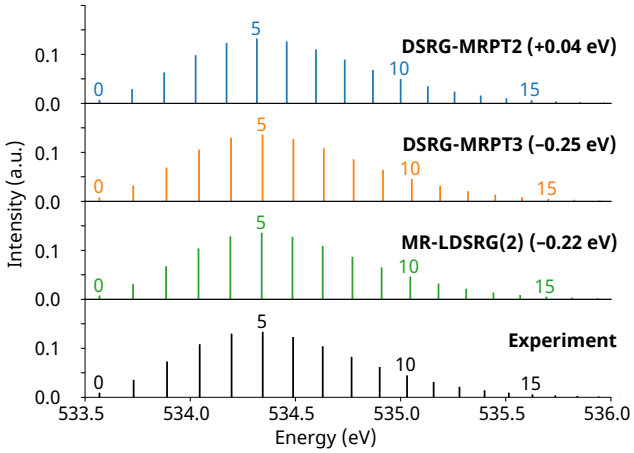

Figure 4: Spectrum of the CO $1s_O \rightarrow 2\pi$ transition simulated from the potential calculated at the DSRG-MRPT2, DSRG-MRPT3, MR-LDSRG(2) levels of theory using the cc-pCVQZ-DK basis set, as well as the experimentally-determined Morse operator constants. The theoretical spectra are shifted to align the 0–0 transition with experiment. Each transition is labeled with the vibrational quantum number ν' of the upper state.

Table 4: Adiabatic transition energies (in eV) evaluated using the experimental ground and excited state equilibrium geometries for the five diatomic molecules. Results were calculated with different MR-DSRG theories based on a GASSCF reference [PT2 = DSRG-MRPT2, PT3 = DSRG-MRPT3, LDSRG(2) = MR-LDSRG(2)] , CVS-ADC theory [ADC(2) = CVS-ADC(2), ADC(2)-x = CVS-ADC(2)-x, ADC(3) = CVS-ADC(3)] and CVS-EOM-CCSD level of theory using the cc-pCVQZ-DK basis and a spin-free X2C 1-electron treatment of scalar relativistic effects. The ADC adiabatic energies are approximated as the sum of the vertical transition energy at the excited state equilibrium geometry and the ground state energy difference between the ground and excited state equilibrium geometries of the ground state. The ground state energies are evaluated using the corresponding Møller–Plesset perturbation theories [MP2 for ADC(2) and ADC(2)-x, MP3 for ADC(3)].

Excitation	T_e(Exp.)	Error(DSRG)			Error(ADC)			Error(EOMCC)
		PT2	PT3	LDSRG(2)	ADC(2)	ADC(2)-x	ADC(3)	CCSD
CO, $1s_C \rightarrow 2\pi$	287.41[a]	0.03	0.32	0.33	2.74	−0.42	0.56	0.77
CO, $1s_O \rightarrow 2\pi$	533.62[b]	−0.04	0.25	0.22	0.78	−1.92	6.25	2.23
N_2, $1\sigma_u \rightarrow 3\sigma_g$	400.76[c]	0.13	0.72	0.62	2.81	−1.24	2.17	1.31
CO^+, $1s_C \rightarrow 5\sigma$	282.00[d]	0.34	0.25	0.20	1.83	−0.46	−0.14	0.52
CO^+, $1s_C \rightarrow 2\pi$(L)	289.85[d]	0.10	0.36	0.35	0.92	−2.22	−1.27	−0.88
CO^+, $1s_O \rightarrow 5\sigma$	528.48[d]	0.49	0.44	0.36	3.82	0.20	7.37	3.05
CO^+, $1s_O \rightarrow 2\pi$(L)	533.44[d]	0.36	0.54	0.51	1.75	−1.72	1.76	1.64
N_2^+, $1\sigma_u \rightarrow 3\sigma_g$	394.28[e]	0.24	0.36	0.25	2.09	−1.54	1.21	0.61
N_2^+, $1\sigma_u \rightarrow 1\pi_g$(L)	402.24[e]	−0.22	0.23	0.19	1.84	−2.17	0.97	0.42
N_2^+, $1\sigma_u \rightarrow 1\pi_g$(H)	403.11[e]	0.19	0.69	0.63	2.31	−2.04	1.81	0.81
NO, $1s_N \rightarrow 2\pi(^2\Delta)$	399.40[f]	0.15	0.31	0.28	1.63	−2.00	−0.48	−0.19
NO, $1s_N \rightarrow 2\pi(^2\Sigma^-)$	399.69[f]	0.22	0.40	0.37	3.06	−0.89	1.09	0.94
NO, $1s_N \rightarrow 2\pi(^2\Sigma^+)$	400.01[f]	0.14	0.33	0.30	2.91	−0.98	0.72	0.77
NO, $1s_O \rightarrow 2\pi(^2\Sigma^-)$	531.53[b]	−0.01	0.10	0.06	0.90	−2.42	4.45	1.46
NO, $1s_O \rightarrow 2\pi(^2\Delta)$	532.64[b]	0.02	0.13	0.08	0.55	−2.91	4.22	1.17
NO, $1s_O \rightarrow 2\pi(^2\Sigma^+)$	533.56[b]	0.00	0.19	0.14	0.50	−2.61	5.20	1.81
MAE		0.17	0.35	0.31	1.90	1.61	2.48	1.16
MSE		0.05	0.15	0.29	4.55	3.23	10.96	1.86

[a] From Ref. 121.
[b] From Ref. 123.
[c] From Ref. 129.
[d] From Ref. 80.
[e] From Ref. 81.
[f] From Ref. 124.

Table 5: Selected adiabatic energy splittings (in eV) between core-excited states reported as deviations from the experiment values. Results were calculated with a GASSCF reference and various levels of theory [PT2 = DSRG-MRPT2, PT3 = DSRG-MRPT3, LDSRG(2) = MR-LDSRG(2)] using the cc-pCVQZ-DK basis and a spin-free X2C 1-electron treatment of scalar relativistic effects.

Splitting	ΔT_e(Exp.)	Error(GASSCF)	Error(DSRG)		
			PT2	PT3	LDSRG(2)
CO^+,$1s_C^1 5\sigma^2 - 1s_C^1 5\sigma^1 2\pi^1$(L)	7.85[a]	0.63	–0.24	0.11	0.15
CO^+,$1s_O^1 5\sigma^2 - 1s_O^1 5\sigma^1 2\pi^1$(L)	4.96[a]	0.75	–0.13	0.10	0.15
N_2^+,$1\sigma_u^1 3\sigma_g^2 - 1\sigma_u^1 3\sigma_g^1 1\pi_g^1$(L)	7.96[b]	0.57	–0.46	–0.13	–0.06
N_2^+,$1\sigma_u^1 3\sigma_g^2 - 1\sigma_u^1 3\sigma_g^1 1\pi_g^1$(H)	8.83[b]	1.20	–0.05	0.33	0.38
N_2^+,$1\sigma_u^1 3\sigma_g^1 1\pi_g^1$(L) $- 1\sigma_u^1 3\sigma_g^1 1\pi_g^1$(H)[c]	0.87[b]	0.63	0.41	0.46	0.50
NO,$1s_N^1 2\pi^2(^2\Delta) - 1s_N^1 2\pi^2(^2\Sigma^-)$	0.29[d]	0.04	0.07	0.09	0.09
NO,$1s_N^1 2\pi^2(^2\Delta) - 1s_N^1 2\pi^2(^2\Sigma^+)$	0.61[d]	–0.12	–0.01	0.02	0.02
NO,$1s_O^1 2\pi^2(^2\Sigma^-) - 1s_O^1 2\pi^2(^2\Delta)$	1.11[e]	0.39	0.03	0.03	0.02
NO,$1s_O^1 2\pi^2(^2\Sigma^-) - 1s_O^1 2\pi^2(^2\Sigma^+)$	2.03[e]	0.18	0.01	0.09	0.08
MAE		0.49	0.13	0.11	0.12
MSE		0.37	0.04	0.02	0.03

[a] From Ref. 80.
[b] From Ref. 81.
[c] Not included in MAE or MSE evaluation.
[d] From Ref. 124.
[e] From Ref. 123.

Moving beyond the the electronic structure near the equilibrium geometry, we investigate the overall quality of the potential energy surface by calculating vibrational spectra of all electronic transitions in the test set. As an example, in Figure 4 we report the vibrational spectra of the CO $1s_O \rightarrow 2\pi$ transition calculated from the potential energy surfaces shown in Figure 3. In the bottom panel of Figure 4, we report a comparison with the vibrational spectrum obtained from Morse potentials fitted to experiment.[123] Furthermore, the theoretical traces are shifted to align the 0–0 transition to the experimental one. The intensity in all these traces are normalized so that the sum of the Franck–Condon factors is equal to 1. Due to the relatively large difference between the ground and excited state equilibrium geometries, the vibrational transitions of this core-excited transitions populate vibrational states up to $\nu' = 15$ and the band is more than 2 eV wide. In general, all MR-DSRG levels of

theory are in excellent agreement with the frequencies derived from experiment. The most intense peak, found at $\nu' = 5$, is predicted correctly by all GASSCF-MR-DSRG theories. For the most intense part of this vibrational pattern ($\nu' = 0$–10), the DSRG-MRPT3 and MR-LDSRG(2) predict frequencies that are in better agreement with the experimentally-derived ones. However, for larger ν' values, there is slightly better agreement between the DSRG-MRPT2 results and the experimentally derived frequencies.

Table 6: The average vibrational frequency difference with respect to the experiment (in meV). Results were calculated with a GASSCF-MR-DSRG theories [PT2 = DSRG-MRPT2, PT3 = DSRG-MRPT3, LDSRG(2) = MR-LDSRG(2)] using the cc-pCVQZ-DK basis and a spin-free X2C 1-electron treatment of scalar relativistic effects.

Excitation	ν'_{t}	$\Delta\bar{\omega}$(DSRG)		
		PT2	PT3	LDSRG(2)
CO, $1s_C \rightarrow 2\pi$	2	2	3	2
CO, $1s_O \rightarrow 2\pi$	13	25	14	12
N_2, $1\sigma_u \rightarrow 3\sigma_g$	5	17	2	5
CO^+, $1s_C \rightarrow 5\sigma$	2	12	5	5
CO^+, $1s_C \rightarrow 2\pi$(L)	2	10	5	6
CO^+, $1s_O \rightarrow 5\sigma$	2	10	4	2
CO^+, $1s_O \rightarrow 2\pi$(L)	6	30	12	16
$N_2{}^+$, $1\sigma_u \rightarrow 3\sigma_g$	2	11	1	1
$N_2{}^+$, $1\sigma_u \rightarrow 1\pi_g$(L)	3	6	11	11
$N_2{}^+$, $1\sigma_u \rightarrow 1\pi_g$(H)	7	53	38	34
NO, $1s_N \rightarrow 2\pi(^2\Delta)$	8	41	16	19
NO, $1s_N \rightarrow 2\pi(^2\Sigma^-)$	6	36	8	11
NO, $1s_N \rightarrow 2\pi(^2\Sigma^+)$	6	44	11	14
NO, $1s_O \rightarrow 2\pi(^2\Sigma^-)$	4	5	13	14
NO, $1s_O \rightarrow 2\pi(^2\Delta)$	4	5	4	5
NO, $1s_O \rightarrow 2\pi(^2\Sigma^+)$	5	3	8	9
All lines	77	25	12	13

To quantify the quality of the vibrational spectra for all the molecules considered, we evaluate two metrics: i) the averaged vibrational frequency difference, and ii) the intensity ratio. The former is reported in Table 6, while the latter is reported in Table **??** and discussed in the Supplementary Information. The average vibrational frequency difference, $\Delta\bar{\omega}$, is defined as

$$\Delta\bar{\omega} = \frac{1}{\nu'_{\mathrm{max}}} \sum_{\nu'=1}^{\nu'_{\mathrm{max}}} |f^{\mathrm{DSRG}}_{0\rightarrow\nu'} - f^{\mathrm{exp}}_{0\rightarrow\nu'}|, \tag{8}$$

where $f_{0\rightarrow\nu'}$ are line positions for the transition from the $\nu'' = 0$ vibrational state of the

ground electronic state and the ν' vibrational state of the core-excited state. The quantity ν'_{max} is the highest quantum number used in the averaging, and is chosen as the larges ν' with corresponding normalized intensity ($I_{0\to\nu'}$) greater than 0.01. The resulting $\Delta\bar{\omega}$ is 25 meV for the DSRG-MRPT2 level of theory, and only 14 and 12 meV for the DSRG-MRPT3 and MR-LDSRG(2) theories. Under this metric, the DSRG-MRPT3 and MR-LDSRG(2) theories lead to a significant improvement in terms of agreement with the experiment. This trend is also true for nearly all the transitions, as it can be seen in Table 6. For N_2, CO^+ and the nitrogen K-edge of NO, this improvement in accuracy is even more significant.

The only case where GASSCF-MR-DSRG theories deviate significantly from the experimentally derived vibrational frequencies is the $1\sigma_u^1 3\sigma_g^1 1\pi_g^1$ (H) state of $N_2{}^+$. SA-RASPT2[81] accurately predicts the 0.87 eV splitting between the $1\sigma_u^1 3\sigma_g^1 1\pi_g^1$ (H)/(L) states (0.91 eV from theory), and it yields harmonic frequencies [212.15 and 214.53 meV for (H)/(L)] for the two states that agree relatively well with their experimental values [218.8 and 215.4 meV for (H)/(L)]. However, a key difference between the SA-RASPT2 calculation and our results is the use of a larger active space consisting of 13 orbitals and averaged over 24 states, which suggests that the accurate prediction of each state may be sensitive to the details in the selection of active space and state-averaging.

To investigate the effect of active space in this molecule, we performed GASSCF-MR-DSRG calculations for $N_2{}^+$ with a larger active space (2o,3e;11o,6e). The corresponding ground state calculations are also performed with the GAS space (2o,4e;11o,5e). Figure 5 shows the potential energy curves of the $1\sigma_u^1 3\sigma_g^1 1\pi_g^1$ (H) and (L) states using two different active spaces and the corresponding orbitals. The potential energy plots show that the splittings between the $1\sigma_u^1 3\sigma_g^1 1\pi_g^1$ (L) and (H) states decreases significantly around the equilibrium region of two potentials in the larger active space. The adiabatic energy splittings between these two states are 0.94, 0.97, and 0.96 eV for the DSRG-MRPT2, DSRG-MRPT3, and MR-LDSRG(2) level of theories, respectively, values that are much closer to experiment (0.87 eV) than the values obtained with the smaller active space (1.28–1.37 eV, reported

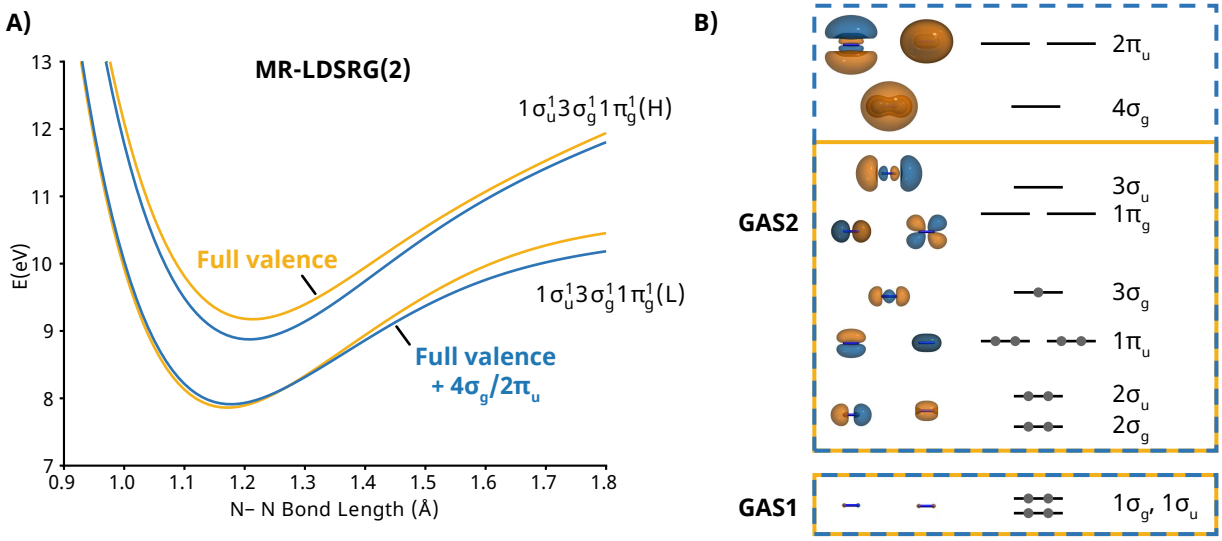

Figure 5: Molecular orbitals used for the GASSCF calculations. A) The potential energy surface for the $1\sigma_u^1 3\sigma_g^1 1\pi_g^1$ (L) and $1\sigma_u^1 3\sigma_g^1 1\pi_g^1$ (H) states of N_2^+ calculated using GASSCF-MR-DSRG level of theory and cc-pCVQZ-DK basis. The solid and dashed lines are calculated with the general (2o, 3e; 8o, 6e) and enlarged (2o, 3e; 11o, 6e) active spaces, respectively. All the curves are shifted so that the value of MR-LDSRG(2) potential energy for $1\sigma_u^1 3\sigma_g^2$ state (the lowest K-edge core-excited state) at its minimum is zero. B) Orbitals and ground state electronic configuration of N_2^+. The orbitals surrounded by solid and dashed lines are included in the full valence (2o,3e;8o,6e) and enlarged (2o,3e;11o, 6e) active spaces, respectively.

in Table 5). The vibrational features of these two states are also well reproduced as the $\Delta\bar{\omega}$ values for the $1\sigma_u^1 3\sigma_g^1 1\pi_g^1$ (H) state decrease to 24, 3, and 4 meV for DSRG-MRPT2, DSRG-MRPT3, MR-LDSRG(2) level of theory, respectively, improving significantly upon the values reported in Table 6 (53, 38, and 34 meV, respectively). Similar improvements are observed for the $\Delta\bar{\omega}$ value of the $1\sigma_u^1 3\sigma_g^1 1\pi_g^1$ (L) state across all MR-DSRG theories.

In terms of the wave function, at the experimental ground state geometry (1.116 Å) the leading contributions from a full valence active space GASSCF-MR-LDSRG(2) calculation to the $1\sigma_u^1 3\sigma_g^1 1\pi_g^1$ (L) state are the configurations

$$
\begin{aligned}
|\Phi_1\rangle &= |1\sigma_g^2 1\sigma_u^1 2\sigma_g^2 2\sigma_u^2 1\pi_u^4 3\sigma_g^1 1\pi_g^1\rangle \\
|\Phi_2\rangle &= |1\sigma_g^1 1\sigma_u^2 2\sigma_g^2 2\sigma_u^1 1\pi_u^4 3\sigma_g^2 1\pi_g^1\rangle
\end{aligned}
\tag{9}
$$

with weights equal to 60% and 20%, respectively. In the large active space calculation the contributions of these two terms is nearly unchanged, with weights of 60% and 17%, respectively. Similarly, the leading terms in the $1\sigma_u^1 3\sigma_g^1 1\pi_g^1$ (H) state are $|\Phi_1\rangle$ (71%) and the following doubly excited configuration (5%)

$$|\Phi_3\rangle = |1\sigma_g^1 1\sigma_u^2 2\sigma_g^2 2\sigma_u^2 1\pi_u^3 3\sigma_g^1 1\pi_g^2\rangle \tag{10}$$

with nearly identical weights in the full valence and the larger active space. Although increasing the size of the active space does not introduce significant difference in terms of CI coefficient, the improved energetics and frequencies are consistent with the general improvement of MCSCF results with active space size.[130] As previously observed in a SA-RASPT2 study,[81] an important role is played by the doubly excited configurations Φ_2 and Φ_3 that involve the $2\sigma_u$ and $1\pi_u$ orbitals. For example, if we constrain the number of electrons in the $2\sigma_g/2\sigma_u$ orbitals to 2, the vertical splitting between the H and L states reduces significantly from 1.58 to 0.59 eV.

5 Conclusions

This study explores a multireference approach for computing core-excited electronic states based on the driven similarity renormalization group (DSRG). Core-excited states are modeled at zeroth-order by a generalized-active-space self-consistent-field reference, followed by a treatment of dynamical electron correlation via a perturbative or iterative MR-DSRG approach. We first investigated how the choice of basis functions and the DSRG flow parameter affect the accuracy of core-excitation energies. Three GASSCF-MR-DSRG approaches are then used to simulate the vibrationally-resolved K-edge X-ray absorption spectra of C, N, and O atoms in five diatomic molecules. The computed adiabatic electronic energies and the vibrational structure of these transitions are in good agreement with experimental results and are comparable with other multireference methods such as RASPT2[80,81] and inner-shell

CASSCF-MCCEPA.[82,123] Third- and high-order terms bring significant improvements in the potential energy curves along dissociative pathways. For example, going beyond second-order perturbation theory, the calculated vibrational spectra agree better with the experimental ones, halving the average vibrational frequency errors to below 15 meV. We additionally investigate the effect of active space choices for the $1\sigma_u^1 3\sigma_g^1 1\pi_g^1$ (H) and (L) states N_2^+, where augmenting the full valence space with additional 3s σ and 3p π orbitals in the GAS2 space is crucial to obtain accurate excitation energies and vibrational frequencies.

This study points towards two major advantages of state-specific multireference strategies, like the GASSCF-MR-DSRG, when it comes to modeling core-excited states. Firstly, they can be applied to multideterminantal states that arise in bond-breaking processes, open-shell states, and multi-electron excitations, avoiding some limitations of single-reference formalisms. For example, ground and core-excited states GASSCF-MR-DSRG potential energy curves are qualitatively and quantitatively accurate along dissociation pathways. Furthermore, excited states with multi-electron character, like the H/L $1\sigma_u^1 3\sigma_g^1 1\pi_g^1$ states of N_2^+, can be accurately modeled already using GASSCF-MR-DSRG second-order perturbation theory. Secondly, the variational treatment of the dominant contributions to core-excitation energies (reference-relaxation and static correlation) leads to a balanced treatment of the electronic structure, as reflected in the high accuracy of the excitation energies computed in this work. Such a strategy reduces the burden on the MR-DSRG to correct the wave function and yields excitation energies that are already in excellent agreement at second-order and converge rapidly with the inclusion of higher-order dynamical correlation effects.

Despite their advantages, there are two aspects of the current state-specific approach that merit further developments. The first one is evaluating transition intensities. While there are challenges associated with computing matrix elements of the dipole operator between two state-specific MR-DSRG solutions, we expect that the leading contribution could be captured by matrix elements of the GASSCF reference states, augmented with low-order corrections. A second challenge is extending computations beyond the first few low-lying

core-excited states, and that we expect could be achieved by introducing elements of state-averaged formalisms.

In the future, we envision several developments of the GASSCF-MR-DSRG approach. We expect that the balance of low cost and relatively high accuracy of the GASSCF-DSRG-MRPT2 level of theory could provide a viable method to compute core-excited states in larger open-shell systems like transition metal complexes. Another interesting extension of the present formalism is the computation of core-excitation of valence-excited states, which would enable the application of these methods to the X-ray spectroscopy of transient species.

Acknowledgement

The authors would like to thank Lan Cheng for providing the code used to generate the CVS-EOM-CCSD results reported in this paper. This research was supported by the U.S. National Science Foundation under award number CHEM-1900532.

6 Supporting Information

See supporting information for additional calculations on the transitions in our preliminary test set: 1) The splittings between adiabatic electronic energies evaluated using ADC and EOMCC theories 2) Relative vibrational intensities calculated from the GASSCF-MRDSRG theories 3) The Morse potential parameters obtained from fitting the GASSCF-MRDSRG potential energy surfaces This information is available free of charge via the Internet at http://pubs.acs.org.

A Expressions of the DSRG source operator

The DSRG source operator $\hat{R}(s)$ can be written as sum of normal ordered many-body operators of different rank

$$\hat{R}(s) = \hat{R}_1(s) + \hat{R}_2(s) + \cdots \tag{11}$$

where $\hat{R}_k(s)$ can be written as

$$\hat{R}_k(s) = \frac{1}{(k!)^2} \sum_{ij\cdots} \sum_{ab\cdots} r^{ij\cdots}_{ab\cdots}(s)(\{\hat{a}^{ij\cdots}_{ab\cdots}\} + \{\hat{a}^{ab\cdots}_{ij\cdots}\}) \tag{12}$$

and

$$r^{ij\cdots}_{ab\cdots}(s) = [\bar{H}^{ij\cdots}_{ab\cdots}(s) + t^{ij\cdots}_{ab\cdots}(s)\Delta^{ij\cdots}_{ab\cdots}]e^{-s(\Delta^{ij\cdots}_{ab\cdots})^2} \tag{13}$$

In these equations, $\bar{H}^{ij\cdots}_{ab\cdots}(s)$ is a rank $2k$ tensor associated with the k-body operator of $\bar{H}^N(s)$. The cluster amplitude $t^{ij\cdots}_{ab\cdots}(s)$ corresponds to excitations from orbitals $i, j, \cdots$ to orbitals $a, b, \cdots$. The quantity $\Delta^{ij\cdots}_{ab\cdots} = \epsilon_a + \epsilon_b + \cdots - \epsilon_i - \epsilon_j - \cdots$ is the generalized Møller–Plesset denominator defined in terms of the semicanonical orbital energies ϵ_p.

References

(1) Kraus, P. M.; Zürch, M.; Cushing, S. K.; Neumark, D. M.; Leone, S. R. The ultrafast X-ray spectroscopic revolution in chemical dynamics. *Nat. Rev. Chem.* **2018**, *2*, 82–94.

(2) Bhattacherjee, A.; Leone, S. R. Ultrafast X-ray Transient Absorption Spectroscopy of Gas-Phase Photochemical Reactions: A New Universal Probe of Photoinduced Molecular Dynamics. *Acc. Chem. Res.* **2018**, *51*, 3203–3211.

(3) Nisoli, M.; Decleva, P.; Calegari, F.; Palacios, A.; Martín, F. Attosecond Electron Dynamics in Molecules. *Chem. Rev.* **2017**, *117*, 10760–10825.

(4) Attar, A. R.; Bhattacherjee, A.; Pemmaraju, C. D.; Schnorr, K.; Closser, K. D.;

Prendergast, D.; Leone, S. R. Femtosecond x-ray spectroscopy of an electrocyclic ring-opening reaction. *Science* **2017**, *356*, 54–59.

(5) Loh, Z. H.; Doumy, G.; Arnold, C.; Kjellsson, L.; Southworth, S. H.; Al Haddad, A.; Kumagai, Y.; Tu, M. F.; Ho, P. J.; March, A. M.; Schaller, R. D.; Bin Mohd Yusof, M. S.; Debnath, T.; Simon, M.; Welsch, R.; Inhester, L.; Khalili, K.; Nanda, K.; Krylov, A. I.; Moeller, S.; Coslovich, G.; Koralek, J.; Minitti, M. P.; Schlotter, W. F.; Rubensson, J. E.; Santra, R.; Young, L. Observation of the fastest chemical processes in the radiolysis of water. *Science* **2020**, *367*, 179–182.

(6) Pertot, Y.; Schmidt, C.; Matthews, M.; Chauvet, A.; Huppert, M.; Svoboda, V.; Von Conta, A.; Tehlar, A.; Baykusheva, D.; Wolf, J. P.; Wörner, H. J. Time-resolved x-ray absorption spectroscopy with a water window high-harmonic source. *Science* **2017**, *355*, 264–267.

(7) Chen, C. T.; Ma, Y.; Sette, F. K-shell photoabsorption of the N_2 molecule. *Phys. Rev. A* **1989**, *40*, 6737–6740.

(8) Ma, Y.; Chen, C. T.; Meigs, G.; Randall, K.; Sette, F. High-resolution K-shell photoabsorption measurements of simple molecules. *Phys. Rev. A* **1991**, *44*, 1848–1858.

(9) Norman, P.; Dreuw, A. Simulating X-ray Spectroscopies and Calculating Core-Excited States of Molecules. *Chem. Rev.* **2018**, *118*, 7208–7248.

(10) Rankine, C. D.; Penfold, T. J. Progress in the Theory of X-ray Spectroscopy: From Quantum Chemistry to Machine Learning and Ultrafast Dynamics. *J. Phys. Chem. A* **2021**, *125*, 4276–4293.

(11) Jenkins, A. J.; Liu, H.; Kasper, J. M.; Frisch, M. J.; Li, X. Variational Relativistic Two-Component Complete-Active-Space Self-Consistent Field Method. *J. Chem. Theory Comput.* **2019**, *15*, 2974–2982.

(12) Hu, H.; Jenkins, A. J.; Liu, H.; Kasper, J. M.; Frisch, M. J.; Li, X. Relativistic Two-Component Multireference Configuration Interaction Method with Tunable Correlation Space. *J. Chem. Theory Comput.* **2020**, *16*, 2975–2984.

(13) Cheng, L. A study of non-iterative triples contributions in relativistic equation-of-motion coupled-cluster calculations using an exact two-component Hamiltonian with atomic mean-field spin-orbit integrals: Application to uranyl and other heavy-element compounds. *J. Chem. Phys.* **2019**, *151*, 1–9.

(14) Liu, J.; Cheng, L. Relativistic coupled-cluster and equation-of-motion coupled-cluster methods. *WIREs Comput. Mol. Sci.* **2021**, 1–21.

(15) Schmitt, A.; Schirmer, J. Molecular K-shell excitation spectra in the relaxed-core Hartree-Fock approximation. *Chem. Phys.* **1992**, *164*, 1–9.

(16) Gilbert, A. T.; Besley, N. A.; Gill, P. M. Self-consistent field calculations of excited states using the maximum overlap method (MOM). *J. Phys. Chem. A* **2008**, *112*, 13164–13171.

(17) Besley, N. A.; Gilbert, A. T.; Gill, P. M. Self-consistent-field calculations of core excited states. *J. Chem. Phys.* **2009**, *130*.

(18) Derricotte, W. D.; Evangelista, F. A. Simulation of X-ray absorption spectra with orthogonality constrained density functional theory. *Phys. Chem. Chem. Phys.* **2015**, *17*, 14360–14374.

(19) Hait, D.; Haugen, E. A.; Yang, Z.; Oosterbaan, K. J.; Leone, S. R.; Head-Gordon, M. Accurate prediction of core-level spectra of radicals at density functional theory cost via square gradient minimization and recoupling of mixed configurations. *J. Chem. Phys.* **2020**, *153*.

(20) Hait, D.; Head-Gordon, M. Highly Accurate Prediction of Core Spectra of Molecules at Density Functional Theory Cost: Attaining Sub-electronvolt Error from a Restricted Open-Shell Kohn-Sham Approach. *J. Phys. Chem. Lett.* **2020**, *11*, 775–786.

(21) Stener, M.; Fronzoni, G.; de Simone, M. Time dependent density functional theory of core electrons excitations. *Chem. Phys. Lett.* **2003**, *373*, 115–123.

(22) Nakata, A.; Imamura, Y.; Nakai, H. Extension of the core-valence-Rydberg B3LYP functional to core-excited-state calculations of third-row atoms. *J. Chem. Theory Comput.* **2007**, *3*, 1295–1305.

(23) Ekström, U.; Norman, P.; Carravetta, V.; Ågren, H. Polarization propagator for X-ray spectra. *Phys. Rev. Lett.* **2006**, *97*, 2–5.

(24) Song, J. W.; Watson, M. A.; Nakata, A.; Hirao, K. Core-excitation energy calculations with a long-range corrected hybrid exchange-correlation functional including a short-range Gaussian attenuation (LCgau-BOP). *J. Chem. Phys.* **2008**, *129*.

(25) Besley, N. A.; Peach, M. J.; Tozer, D. J. Time-dependent density functional theory calculations of near-edge X-ray absorption fine structure with short-range corrected functionals. *Phys. Chem. Chem. Phys.* **2009**, *11*, 10350–10358.

(26) Besley, N. A. Fast Time-Dependent Density Functional Theory Calculations of the X-ray Absorption Spectroscopy of Large Systems. *J. Chem. Theory Comput.* **2016**, *12*, 5018–5025.

(27) Liang, W.; Fischer, S. A.; Frisch, M. J.; Li, X. Energy-specific linear response TDHF/TDDFT for calculating high-energy excited states. *J. Chem. Theory Comput.* **2011**, *7*, 3540–3547.

(28) Zhang, Y.; Biggs, J. D.; Healion, D.; Govind, N.; Mukamel, S. Core and valence

excitations in resonant X-ray spectroscopy using restricted excitation window time-dependent density functional theory. *J. Chem. Phys.* **2012**, *137*.

(29) Lestrange, P. J.; Nguyen, P. D.; Li, X. Calibration of Energy-Specific TDDFT for Modeling K-edge XAS Spectra of Light Elements. *J. Chem. Theory Comput.* **2015**, *11*, 2994–2999.

(30) Triguero, L.; Pettersson, L.; Ågren, H. Calculations of near-edge x-ray-absorption spectra of gas-phase and chemisorbed molecules by means of density-functional and transition-potential theory. *Phys. Rev. B: Condens. Matter Mater. Phys.* **1998**, *58*, 8097–8110.

(31) Leetmaa, M.; Ljungberg, M. P.; Lyubartsev, A.; Nilsson, A.; Pettersson, L. G. Theoretical approximations to X-ray absorption spectroscopy of liquid water and ice. *J. Electron Spectrosc. Relat. Phenom.* **2010**, *177*, 135–157.

(32) Ågren, H.; Carravetta, V.; Vahtras, O.; Pettersson, L. G. Direct SCF direct static-exchange calculations of electronic spectra. *Theor. Chem. Acc.* **1997**, *97*, 14–40.

(33) Ekström, U.; Norman, P.; Carravetta, V. Relativistic four-component static-exchange approximation for core-excitation processes in molecules. *Phys. Rev. A: At., Mol., Opt. Phys.* **2006**, *73*, 1–9.

(34) Asmuruf, F. A.; Besley, N. A. Calculation of near-edge X-ray absorption fine structure with the CIS(D) method. *Chem. Phys. Lett.* **2008**, *463*, 267–271.

(35) Roemelt, M.; Maganas, D.; Debeer, S.; Neese, F. A combined DFT and restricted open-shell configuration interaction method including spin-orbit coupling: Application to transition metal L-edge X-ray absorption spectroscopy. *J. Chem. Phys.* **2013**, *138*.

(36) Maganas, D.; Roemelt, M.; Hävecker, M.; Trunschke, A.; Knop-Gericke, A.; Schlögl, R.; Neese, F. First principles calculations of the structure and V L-edge X-ray

absorption spectra of V_2O_5 using local pair natural orbital coupled cluster theory and spin–orbit coupled configuration interaction approaches. *Phys. Chem. Chem. Phys.* **2013**, *15*, 7260.

(37) Maganas, D.; Debeer, S.; Neese, F. Pair Natural Orbital Restricted Open-Shell Configuration Interaction (PNO-ROCIS) Approach for Calculating X-ray Absorption Spectra of Large Chemical Systems. *J. Phys. Chem. A* **2018**, *122*, 1215–1227.

(38) Oosterbaan, K. J.; White, A. F.; Head-Gordon, M. Non-orthogonal configuration interaction with single substitutions for the calculation of core-excited states. *J. Chem. Phys.* **2018**, *149*.

(39) Oosterbaan, K. J.; White, A. F.; Head-Gordon, M. Non-Orthogonal Configuration Interaction with Single Substitutions for Core-Excited States: An Extension to Doublet Radicals. *J. Chem. Theory Comput.* **2019**, *15*, 2966–2973.

(40) Garner, S. M.; Neuscamman, E. Core excitations with excited state mean field and perturbation theory. *J. Chem. Phys.* **2020**, *153*.

(41) Coriani, S.; Christiansen, O.; Fransson, T.; Norman, P. Coupled-cluster response theory for near-edge x-ray-absorption fine structure of atoms and molecules. *Phys. Rev. A: At., Mol., Opt. Phys.* **2012**, *85*, 1–8.

(42) Coriani, S.; Fransson, T.; Christiansen, O.; Norman, P. Asymmetric-lanczos-chain-driven implementation of electronic resonance convergent coupled-cluster linear response theory. *J. Chem. Theory Comput.* **2012**, *8*, 1616–1628.

(43) Coriani, S.; Koch, H. Communication: X-ray absorption spectra and core-ionization potentials within a core-valence separated coupled cluster framework. *J. Chem. Phys.* **2015**, *143*.

(44) Faber, R.; Coriani, S. Resonant Inelastic X-ray Scattering and Nonesonant X-ray Emission Spectra from Coupled-Cluster (Damped) Response Theory. *J. Chem. Theory Comput.* **2019**, *15*, 520–528.

(45) Faber, R.; Coriani, S. Core-valence-separated coupled-cluster-singles-and-doubles complex-polarization-propagator approach to X-ray spectroscopies. *Phys. Chem. Chem. Phys.* **2020**, *22*, 2642–2647.

(46) Nooijen, M.; Bartlett, R. J. Description of core-excitation spectra by the open-shell electron-attachment equation-of-motion coupled cluster method. *J. Chem. Phys.* **1995**, *102*, 6735–6756.

(47) Peng, B.; Lestrange, P. J.; Goings, J. J.; Caricato, M.; Li, X. Energy-Specific Equation-of-Motion Coupled-Cluster Methods for High-Energy Excited States: Application to K-edge X-ray Absorption Spectroscopy. *J. Chem. Theory Comput.* **2015**, *11*, 4146–4153.

(48) Vidal, M. L.; Feng, X.; Epifanovsky, E.; Krylov, A. I.; Coriani, S. New and Efficient Equation-of-Motion Coupled-Cluster Framework for Core-Excited and Core-Ionized States. *J. Chem. Theory Comput.* **2019**, *15*, 3117–3133.

(49) Vidal, M. L.; Krylov, A. I.; Coriani, S. Dyson orbitals within the fc-CVS-EOM-CCSD framework: theory and application to X-ray photoelectron spectroscopy of ground and excited states. *Phys. Chem. Chem. Phys.* **2020**, *22*, 2693–2703.

(50) Nanda, K. D.; Krylov, A. I. Cherry-picking resolvents: A general strategy for convergent coupled-cluster damped response calculations of core-level spectra. *J. Chem. Phys.* **2020**, *153*.

(51) Folkestad, S. D.; Koch, H. Equation-of-Motion MLCCSD and CCSD-in-HF Oscillator Strengths and Their Application to Core Excitations. *J. Chem. Theory Comput.* **2020**, *16*, 6869–6879.

(52) Myhre, R. H.; Coriani, S.; Koch, H. Near-Edge X-ray Absorption Fine Structure within Multilevel Coupled Cluster Theory. *J. Chem. Theory Comput.* **2016**, *12*, 2633–2643.

(53) Peng, R.; Copan, A. V.; Sokolov, A. Y. Simulating X-ray Absorption Spectra with Linear-Response Density Cumulant Theory. *J. Phys. Chem. A* **2019**, *123*, 1840–1850.

(54) Wenzel, J.; Wormit, M.; Dreuw, A. Calculating X-ray absorption spectra of open-shell molecules with the unrestricted algebraic-diagrammatic construction scheme for the polarization propagator. *J. Chem. Theory Comput.* **2014**, *10*, 4583–4598.

(55) Wenzel, J.; Wormit, M.; Dreuw, A. Calculating core-level excitations and x-ray absorption spectra of medium-sized closed-shell molecules with the algebraic-diagrammatic construction scheme for the polarization propagator. *J. Comput. Chem.* **2014**, *35*, 1900–1915.

(56) Wenzel, J.; Holzer, A.; Wormit, M.; Dreuw, A. Analysis and comparison of CVS-ADC approaches up to third order for the calculation of core-excited states. *J. Chem. Phys.* **2015**, *142*.

(57) Lopata, K.; Van Kuiken, B. E.; Khalil, M.; Govind, N. Linear-Response and Real-Time Time-Dependent Density Functional Theory Studies of Core-Level Near-Edge X-Ray Absorption. *J. Chem. Theory Comput.* **2012**, *8*, 3284–3292.

(58) Fernando, R. G.; Balhoff, M. C.; Lopata, K. X-ray absorption in insulators with non-hermitian real-time time-dependent density functional theory. *J. Chem. Theory Comput.* **2015**, *11*, 646–654.

(59) Kadek, M.; Konecny, L.; Gao, B.; Repisky, M.; Ruud, K. X-ray absorption resonances near $L_{2,3}$-edges from real-time propagation of the Dirac-Kohn-Sham density matrix. *Phys. Chem. Chem. Phys.* **2015**, *17*, 22566–22570.

(60) Kasper, J. M.; Lestrange, P. J.; Stetina, T. F.; Li, X. Modeling $L_{2,3}$-Edge X-ray Absorption Spectroscopy with Real-Time Exact Two-Component Relativistic Time-Dependent Density Functional Theory. *J. Chem. Theory Comput.* **2018**, *14*, 1998–2006.

(61) Nascimento, D. R.; Deprince, A. E. Simulation of Near-Edge X-ray Absorption Fine Structure with Time-Dependent Equation-of-Motion Coupled-Cluster Theory. *J. Phys. Chem. Lett.* **2017**, *8*, 2951–2957.

(62) Sherrill, C. D.; Dutta, A.; Abrams, M. L.; Sears, J. S. Bond breaking in quantum chemistry: A comparison of single- and multi-reference methods. *ACS Symp. Ser.* **2007**, *958*, 75–88.

(63) Rocha, A. B. Potential curves for inner-shell states of CO calculated at multiconfigurational self-consistent field level. *J. Chem. Phys.* **2011**, *134*, 024107.

(64) Alagia, M.; Bodo, E.; Decleva, P.; Falcinelli, S.; Ponzi, A.; Richter, R.; Stranges, S. The soft X-ray absorption spectrum of the allyl free radical. *Phys. Chem. Chem. Phys.* **2013**, *15*, 1310–1318.

(65) Guo, M.; Sørensen, L. K.; Delcey, M. G.; Pinjari, R. V.; Lundberg, M. Simulations of iron K pre-edge X-ray absorption spectra using the restricted active space method. *Phys. Chem. Chem. Phys.* **2016**, *18*, 3250–3259.

(66) Helmich-Paris, B. Simulating X-ray absorption spectra with complete active space self-consistent field linear response methods. *Int. J. Quantum Chem.* **2021**, *121*, 1–20.

(67) Butscher, W.; Buenker, R. J.; Peyerimhoff, S. D. All-electron CI calculations for core-ionized, core-valence excited and shake-up states of N_2. *Chem. Phys. Lett.* **1977**, *52*, 449–456.

(68) Coe, J. P.; Paterson, M. J. Multireference X-ray emission and absorption spectroscopy calculations from Monte Carlo configuration interaction. *Theor. Chem. Acc.* **2015**, *134*, 3–9.

(69) Lisini, A.; Decleva, P. Calculation of dynamical correlation effects by quasidegenerate perturbation theory. An application to photoionization spectra. *Chem. Phys.* **1992**, *168*, 1–13.

(70) Brabec, J.; Bhaskaran-Nair, K.; Govind, N.; Pittner, J.; Kowalski, K. Communication: Application of state-specific multireference coupled cluster methods to core-level excitations. *J. Chem. Phys.* **2012**, *137*, 1–5.

(71) Sen, S.; Shee, A.; Mukherjee, D. A study of the ionisation and excitation energies of core electrons using a unitary group adapted state universal approach. *Mol. Phys.* **2013**, *111*, 2625–2639.

(72) Dutta, A. K.; Gupta, J.; Vaval, N.; Pal, S. Intermediate Hamiltonian Fock space multireference coupled cluster approach to core excitation spectra. *J. Chem. Theory Comput.* **2014**, *10*, 3656–3668.

(73) Maganas, D.; Kowalska, J. K.; Nooijen, M.; Debeer, S.; Neese, F. Comparison of multireference ab initio wavefunction methodologies for X-ray absorption edges: A case study on $[Fe(II/III)Cl_4]^{2-/1-}$ molecules. *J. Chem. Phys.* **2019**, *150*.

(74) Lyakh, D. I.; Musiał, M.; Lotrich, V. F.; Bartlett, R. J. Multireference Nature of Chemistry: The Coupled-Cluster View. *Chem. Rev.* **2012**, *112*, 182–243.

(75) Köhn, A.; Hanauer, M.; Mück, L. A.; Jagau, T. C.; Gauss, J. State-specific multireference coupled-cluster theory. *Wiley Interdiscip. Rev. Comput. Mol. Sci.* **2013**, *3*, 176–197.

(76) Evangelista, F. A. Perspective: Multireference coupled cluster theories of dynamical electron correlation. *J. Chem. Phys.* **2018**, *149*, 030901.

(77) Malmqvist, P. Å.; Rendell, A.; Roos, B. O. The restricted active space self-consistent-field method, implemented with a split graph unitary group approach. *J. Phys. Chem.* **1990**, *94*, 5477–5482.

(78) Malmqvist, P. Å.; Pierloot, K.; Shahi, A. R. M.; Cramer, C. J.; Gagliardi, L. The restricted active space followed by second-order perturbation theory method: Theory and application to the study of CuO_2 and Cu_2O_2 systems. *J. Chem. Phys.* **2008**, *128*.

(79) Sauri, V.; Serrano-Andrés, L.; Shahi, A. R. M.; Gagliardi, L.; Vancoillie, S.; Pierloot, K. Multiconfigurational second-order perturbation theory restricted active space (RASPT2) method for electronic excited states: A benchmark study. *J. Chem. Theory Comput.* **2011**, *7*, 153–168.

(80) Couto, R. C.; Kjellsson, L.; Ågren, H.; Carravetta, V.; Sorensen, S. L.; Kubin, M.; Bülow, C.; Timm, M.; Zamudio-Bayer, V.; von Issendorff, B.; Lau, J. T.; Söderström, J.; Rubensson, J.-E.; Lindblad, R. The carbon and oxygen K-edge NEXAFS spectra of CO^+. *Phys. Chem. Chem. Phys.* **2020**, *22*, 16215–16223.

(81) Lindblad, R.; Kjellsson, L.; Couto, R. C.; Timm, M.; Bülow, C.; Zamudio-Bayer, V.; Lundberg, M.; Von Issendorff, B.; Lau, J. T.; Sorensen, S. L.; Carravetta, V.; Ågren, H.; Rubensson, J. E. X-Ray Absorption Spectrum of the N_2^+ Molecular Ion. *Phys. Rev. Lett.* **2020**, *124*, 203001.

(82) Fink, R. A theoretical simulation of the $1s \rightarrow 2\pi$ excitation and deexcitation spectra of the NO molecule. *J. Chem. Phys.* **1997**, *106*, 4038–4052.

(83) Josefsson, I.; Kunnus, K.; Schreck, S.; Föhlisch, A.; De Groot, F.; Wernet, P.; Odelius, M. Ab initio calculations of X-ray spectra: Atomic multiplet and molec-

ular orbital effects in a multiconfigurational scf approach to the L-edge spectra of transition metal complexes. *J. Phys. Chem. Lett.* **2012**, *3*, 3565–3570.

(84) Pinjari, R. V.; Delcey, M. G.; Guo, M.; Odelius, M.; Lundberg, M. Restricted active space calculations of L-edge X-ray absorption spectra: From molecular orbitals to multiplet states. *J. Chem. Phys.* **2014**, *141*.

(85) Bokarev, S. I.; Khan, M.; Abdel-Latif, M. K.; Xiao, J.; Hilal, R.; Aziz, S. G.; Aziz, E. F.; Kühn, O. Unraveling the Electronic Structure of Photocatalytic Manganese Complexes by L-Edge X-ray Spectroscopy. *J. Phys. Chem. C* **2015**, *119*, 19192–19200.

(86) Pinjari, R. V.; Delcey, M. G.; Guo, M.; Odelius, M.; Lundberg, M. Cost and sensitivity of restricted active-space calculations of metal L-edge X-ray absorption spectra. *J. Comput. Chem.* **2016**, *37*, 477–486.

(87) Bokarev, S. I.; Dantz, M.; Suljoti, E.; Kühn, O.; Aziz, E. F. State-dependent electron delocalization dynamics at the solute-solvent interface: Soft-x-ray absorption spectroscopy and Ab initio calculations. *Phys. Rev. Lett.* **2013**, *111*, 1–5.

(88) Wernet, P.; Kunnus, K.; Josefsson, I.; Rajkovic, I.; Quevedo, W.; Beye, M.; Schreck, S.; Grübel, S.; Scholz, M.; Nordlund, D.; Zhang, W.; Hartsock, R. W.; Schlotter, W. F.; Turner, J. J.; Kennedy, B.; Hennies, F.; De Groot, F. M.; Gaffney, K. J.; Techert, S.; Odelius, M.; Föhlisch, A. Orbital-specific mapping of the ligand exchange dynamics of $Fe(CO)_5$ in solution. *Nature* **2015**, *520*, 78–81.

(89) Fleig, T.; Olsen, J.; Marian, C. M. The generalized active space concept for the relativistic treatment of electron correlation. I. Kramers-restricted two-component configuration interaction. *J. Chem. Phys.* **2001**, *114*, 4775–4790.

(90) Ma, D.; Li Manni, G.; Gagliardi, L. The generalized active space concept in multiconfigurational self-consistent field methods. *J. Chem. Phys.* **2011**, *135*.

(91) Evangelista, F. A. A driven similarity renormalization group approach to quantum many-body problems. *J. Chem. Phys.* **2014**, *141*.

(92) Li, C.; Evangelista, F. A. Multireference Theories of Electron Correlation Based on the Driven Similarity Renormalization Group. *Annu. Rev. Phys. Chem.* **2019**, *70*, 245–273.

(93) Li, C.; Evangelista, F. A. Driven similarity renormalization group for excited states: A state-averaged perturbation theory. *J. Chem. Phys.* **2018**, *148*, 124106.

(94) Werner, H.-J. Third-order multireference perturbation theory The CASPT3 method. *Mol. Phys.* **1996**, *89*, 645–661.

(95) Grabarek, D.; Walczak, E.; Andruniów, T. Assessing the Accuracy of Various Ab Initio Methods for Geometries and Excitation Energies of Retinal Chromophore Minimal Model by Comparison with CASPT3 Results. *J. Chem. Theory Comput.* **2016**, *12*, 2346–2356.

(96) Li, C.; Evangelista, F. A. Towards numerically robust multireference theories: The driven similarity renormalization group truncated to one- and two-body operators. *J. Chem. Phys.* **2016**, *144*.

(97) Zhang, T.; Li, C.; Evangelista, F. A. Improving the Efficiency of the Multireference Driven Similarity Renormalization Group via Sequential Transformation, Density Fitting, and the Noninteracting Virtual Orbital Approximation. *J. Chem. Theory Comput.* **2019**, *15*, 4399–4414.

(98) Li, C.; Evangelista, F. A. Spin-free implementation of the multireference driven similarity renormalization group: A benchmark study of open-shell diatomic molecules and spin-crossover energetics. 2021.

(99) Li, C.; Evangelista, F. A. Multireference driven similarity renormalization group: A second-order perturbative analysis. *J. Chem. Theory Comput.* **2015**, *11*, 2097–2108.

(100) Li, C.; Evangelista, F. A. Driven similarity renormalization group: Third-order multireference perturbation theory. *J. Chem. Phys.* **2017**, *146*.

(101) Forte, a suite of quantum chemistry methods for strongly correlated electrons. For current version see `https://github.com/evangelistalab/forte`, 2020.

(102) Smith, D. G.; Burns, L. A.; Simmonett, A. C.; Parrish, R. M.; Schieber, M. C.; Galvelis, R.; Kraus, P.; Kruse, H.; Di Remigio, R.; Alenaizan, A.; James, A. M.; Lehtola, S.; Misiewicz, J. P.; Scheurer, M.; Shaw, R. A.; Schriber, J. B.; Xie, Y.; Glick, Z. L.; Sirianni, D. A.; O'Brien, J. S.; Waldrop, J. M.; Kumar, A.; Hohenstein, E. G.; Pritchard, B. P.; Brooks, B. R.; Schaefer, H. F.; Sokolov, A. Y.; Patkowski, K.; Deprince, A. E.; Bozkaya, U.; King, R. A.; Evangelista, F. A.; Turney, J. M.; Crawford, T. D.; Sherrill, C. D. P SI4 1.4: Open-source software for high-throughput quantum chemistry. *J. Chem. Phys.* **2020**, *152*.

(103) Verma, P.; Derricotte, W. D.; Evangelista, F. A. Predicting Near Edge X-ray Absorption Spectra with the Spin-Free Exact-Two-Component Hamiltonian and Orthogonality Constrained Density Functional Theory. *J. Chem. Theory Comput.* **2016**, *12*, 144–156.

(104) Dunning, T. H. Gaussian basis sets for use in correlated molecular calculations. I. The atoms boron through neon and hydrogen. *J. Chem. Phys.* **1989**, *90*, 1007–1023.

(105) De Jong, W. A.; Harrison, R. J.; Dixon, D. A. Parallel Douglas-Kroll energy and gradients in NWChem: Estimating scalar relativistic effects using Douglas-Kroll contracted basis sets. *J. Chem. Phys.* **2001**, *114*, 48–53.

(106) Woon, D. E.; Dunning, T. H. Gaussian basis sets for use in correlated molecular

calculations. V. Core-valence basis sets for boron through neon. *J. Chem. Phys.* **1995**, *103*, 4572–4585.

(107) Kendall, R. A.; Dunning, T. H.; Harrison, R. J. Electron affinities of the first-row atoms revisited. Systematic basis sets and wave functions. *J. Chem. Phys.* **1992**, *96*, 6796–6806.

(108) Weigend, F.; Furche, F.; Ahlrichs, R. Gaussian basis sets of quadruple zeta valence quality for atoms H-Kr. *J. Chem. Phys.* **2003**, *119*, 12753–12762.

(109) Weigend, F.; Ahlrichs, R. Balanced basis sets of split valence, triple zeta valence and quadruple zeta valence quality for H to Rn: Design and assessment of accuracy. *Phys. Chem. Chem. Phys.* **2005**, *7*, 3297–3305.

(110) Roos, B. O.; Lindh, R.; Malmqvist, P. Å.; Veryazov, V.; Widmark, P. O. Main Group Atoms and Dimers Studied with a New Relativistic ANO Basis Set. *J. Phys. Chem. A* **2004**, *108*, 2851–2858.

(111) Lill, J. V.; Parker, G. A.; Light, J. C. Discrete variable representations and sudden models in quantum scattering theory. *Chem. Phys. Lett.* **1982**, *89*, 483–489.

(112) Colbert, D. T.; Miller, W. H. A novel discrete variable representation for quantum mechanical reactive scattering via the S-matrix Kohn method. *J. Chem. Phys.* **1992**, *96*, 1982–1991.

(113) Herbst, M. F.; Scheurer, M.; Fransson, T.; Rehn, D. R.; Dreuw, A. adcc: A versatile toolkit for rapid development of algebraic-diagrammatic construction methods. *Wiley Interdiscip. Rev. Comput. Mol. Sci.* **2020**, *10*, 1–16.

(114) Herbst, M. F.; Scheurer, M.; Drrehn, adc-connect/adcc v0.15.7. 2021.

(115) CFOUR, a quantum chemical program package written by J.F. Stanton, J. Gauss, L. Cheng, M.E. Harding, D.A. Matthews, P.G. Szalaywith contributions from A.A. Auer,

R.J. Bartlett, U. Benedikt, C. Berger, D.E. Bernholdt, S. Blaschke, Y.J. Bomble, S. Burger, O. Christiansen, D. Datta, F. Engel, R. Faber, J. Greiner, M. Heckert, O. Heun, M. Hilgenberg, C. Huber, T.-C. Jagau, D. Jonsson, J. Jusélius, T. Kirsch, K. Klein, G.M. Kopper, W.J. Lauderdale, F. Lipparini, T. Metzroth, L.A. Mück, T. Nottoli, D.P. O'Neill, D.R. Price, E. Prochnow, C. Puzzarini, K. Ruud, F. Schiffmann, W. Schwalbach, C. Simmons, S. Stopkowicz, A. Tajti, J. Vázquez, F. Wang, J.D. Watts and the integral packages MOLECULE (J. Almlöf and P.R. Taylor), PROPS (P.R. Taylor), ABACUS (T. Helgaker, H.J. Aa. Jensen, P. Jørgensen, and J. Olsen), and ECP routines by A. V. Mitin and C. van Wüllen. For the current version, see http://www.cfour.de.

(116) Liu, J.; Matthews, D.; Coriani, S.; Cheng, L. Benchmark Calculations of K-Edge Ionization Energies for First-Row Elements Using Scalar-Relativistic Core–Valence-Separated Equation-of-Motion Coupled-Cluster Methods. *J. Chem. Theory Comput.* **2019**, *15*, 1642–1651.

(117) Matthews, D. A.; Cheng, L.; Harding, M. E.; Lipparini, F.; Stopkowicz, S.; Jagau, T. C.; Szalay, P. G.; Gauss, J.; Stanton, J. F. Coupled-cluster techniques for computational chemistry: The CFOUR program package. *J. Chem. Phys.* **2020**, *152*, 214108.

(118) Chen, C. T.; Sette, F. Performance of the Dragon soft x-ray beamline (invited). *Rev. Sci. Instrum.* **1989**, *60*, 1616–1621.

(119) Svensson, S.; Naves De Brito, A.; Keane, M. P.; Correia, N.; Karlsson, L.; Liegener, C. M.; Ågren, H. S. The N 1s Core Electron Shake-up and the Shake-Up Auger Satellite Spectrum of the N2 Molecule. *Journal of Physics B: Atomic, Molecular and Optical Physics* **1992**, *25*, 135–144.

(120) Neeb, M.; Rubensson, J. E.; Biermann, M.; Eberhardt, W. Coherent excitation of

vibrational wave functions observed in core hole decay spectra of O_2, N_2 and CO. *J. Electron Spectrosc. Relat. Phenom.* **1994**, *67*, 261–274.

(121) Osborne, S. J.; Ausmees, A.; Svensson, S.; Kivimäki, A.; Sairanen, O.; de Brito, A. N.; Aksela, H.; Aksela, S. The vibrationally resolved participator Auger spectra of selectively excited C 1s $(2\sigma)^{-1}$ $2\pi^1$ vibrational states in carbon monoxide. *J. Chem. Phys.* **1995**, *102*, 7317–7324.

(122) Coreno, M.; De Simone, M.; Prince, K. C.; Richter, R.; Vondráček, M.; Avaldi, L.; Camilloni, R. Vibrationally resolved oxygen K $\rightarrow \Pi^*$ spectra of O_2 and CO. *Chem. Phys. Lett.* **1999**, *306*, 269–274.

(123) Püttner, R.; Dominguez, I.; Morgan, T. J.; Cisneros, C.; Fink, R. F.; Rotenberg, E.; Warwick, T.; Domke, M.; Kaindl, G.; Schlachter, A. S. Vibrationally resolved O 1s core-excitation spectra of CO and NO. *Phys. Rev. A: At., Mol., Opt. Phys.* **1999**, *59*, 3415–3423.

(124) Wang, H.; Fink, R. F.; Piancastelli, M. N.; Hjelte, I.; Wiesner, K.; Bässler, M.; Feifel, R.; Björneholm, O.; Miron, C.; Giertz, A.; Burmeister, F.; Sorensen, S. L.; Svensson, S. Filtering core excitation spectra: vibrationally resolved constant ionic state studies of N 1s$\rightarrow 2\pi$ core-excited NO. *J. Phys. B: At., Mol. Opt. Phys.* **2001**, *34*, 4417–4426.

(125) Lofthus, A.; Krupenie, P. H. The spectrum of molecular nitrogen. *J. Phys. Chem. Ref. Data* **1977**, *6*, 113–307.

(126) Varandas, A. J. Extrapolating to the one-electron basis-set limit in electronic structure calculations. *J. Chem. Phys.* **2007**, *126*.

(127) Halkier, A.; Helgaker, T.; Jørgensen, P.; Klopper, W.; Koch, H.; Olsen, J.; Wilson, A. K. Basis-set convergence in correlated calculations on Ne, N_2, and H_2O. *Chem. Phys. Lett.* **1998**, *286*, 243–252.

(128) Helgaker, T.; Klopper, W.; Koch, H.; Noga, J. Basis-set convergence of correlated calculations on water. *J. Chem. Phys.* **1997**, *106*, 9639–9646.

(129) Feifel, R.; Andersson, M.; Öhrwall, G.; Sorensen, S. L.; Piancastelli, M. N.; Tchaplyguine, M.; Björneholm, O.; Karlsson, L.; Svensson, S. A quantitative analysis of the N 1s→π^* photoabsorption profile in N_2: New spectroscopical constants for the core-excited state. *Chem. Phys. Lett.* **2004**, *383*, 222–229.

(130) Andersson, K.; Roos, B. O. Excitation energies in the nickel atom studied with the complete active space SCF method and second-order perturbation theory. *Chem. Phys. Lett.* **1992**, *191*, 507–514.